AD-A107 983 GENERAL ATOMIC CO SAN DIEGO CALIF F/G 20/4
FLUID MECHANICS AND HEAT TRANSFER SPIRALLY FLUTED TUBING,(U)
AUG 81 J C LARUE, P A LIBBY, J S YAMPOLSKY N00014-79-C-0773
UNCLASSIFIED GA-A16541 NL

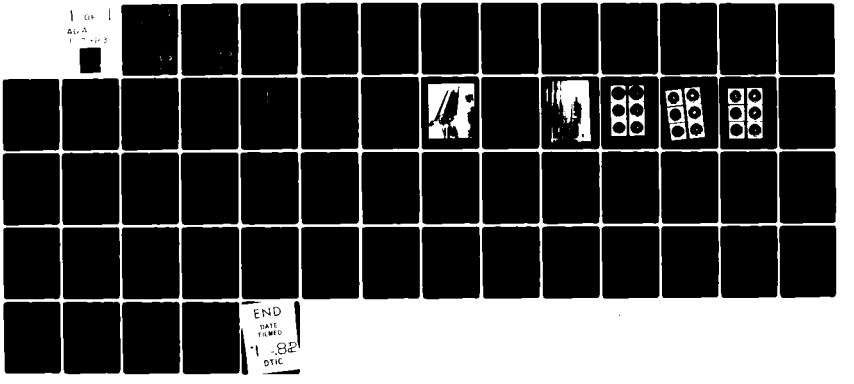

END
DATE FILMED
1 -82
DTIC

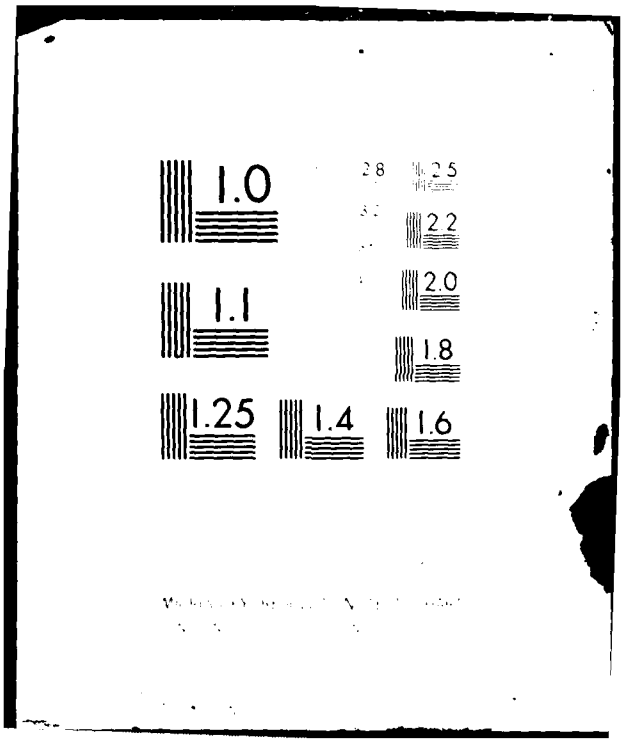
1.0
2.8
2.5
2.2
2.0
1.1
1.8
1.25
1.4
1.6

LEVEL II

12

GA-A16541

FLUID MECHANICS AND HEAT TRANSFER SPIRALLY FLUTED TUBING

by
J. C. LaRUE, P. A. LIBBY, and J. S. YAMPOLSKY

Prepared under
Contract N00014-79-C-0773
for the Office of Naval Research

AUGUST 1981

GENERAL ATOMIC COMPANY

GA-A16541

FLUID MECHANICS AND HEAT TRANSFER SPIRALLY FLUTED TUBING

by

J. C. LaRUE,* P. A. LIBBY,** and J. S. YAMPOLSKY

Prepared under
Contract N00014-79-C-0773
for the Office of Naval Research

*University of California, Irvine, California
**University of California, San Diego, California

GENERAL ATOMIC PROJECT 3774
AUGUST 1981

Original contains color plates: All DTIC reproductions will be in black and white

GENERAL ATOMIC COMPANY

TABLE OF CONTENTS

1. INTRODUCTION AND BACKGROUND

The objective of this program is to develop both a qualitative and a quantitative understanding of the fluid mechanics and heat transfer mechanisms that underlie the measured performance of the spirally fluted tubes under development at General Atomic. The reason for the interest in the spirally fluted tubes is that results to date have indicated three advantages to this tubing concept:

1. The fabrication technique of rolling flutes on strip and subsequently spiralling and simultaneously welding the strip to form tubing results in low fabrication costs, approximately equal to those of commercially welded tubing.

2. The heat transfer coefficient is increased without a concomitant increase of the friction coefficient on the inside of the tube. In single-phase axial flow of water, the helical flutes continuously induce rotation of the flow both within and without the tube as a result of the effect of curvature. This rotation enhances turbulent exchange both on the inside and outside of the tube in the immediate vicinity of the wall. When heat is transferred from a high-temperature fluid external to the tube through the tube wall to a cold fluid within the tube, the density gradients are such as to enhance turbulent exchange in both flows. The improvement in the heat transfer coefficient results from the enhancement of the turbulent exchange.

   An additional effect from rotation of the fluid inside of the tube has been observed for a helix angle of 30°. The friction coefficient does not increase with the increased heat transfer; in fact, it is somewhat lower than that of a smooth round tube at equivalent Reynolds number.

The combination of these two effects results in the achievement of values considerably in excess of one for the ratio of the turbulent exchange coefficients of heat and momentum (the reciprocal of the turbulent Prandtl number). This ratio is equivalent to the ratio of twice the Stanton number, multiplied by the Prandtl number raised to the two-thirds power, to the friction coefficient.

3. An increase in condensation heat transfer on the outside of the tube is achieved. In a vertical orientation with fluid condensing on the outside of the helically fluted tube, the flutes provide a channel for draining the condensed fluid. The surface tension forces draw the condensate film from the crests of the flutes into the troughs. This results in the major portion of the crest having a very thin film, which greatly reduces the resistance to heat flow through the crest area. The result of providing the drainage in the troughs and decreasing the resistance to heat flow over the crests is a substantial improvement in heat transfer performance over conventional smooth tubes. This effect, which was first proposed by Gregorig [1], is not novel to this tubing concept. In fact it is the basis for a number of different proposed enhanced tubes, some of which have straight flutes and some spiralled. However, the combination of this enhancement on the outside of the tube in condensation with the enhancement on the inside of the tube in single-phase water flow can lead to significant improvements in heat transfer performance.

The manufacturing development of the spirally fluted tube is underway and its evaluation will be reported on later. The basis of the other two advantages follow:

1.1 Performance Measurements of Helically Fluted Tubes in Single-Phase Water Flow

The heat transfer performance on the inside of helically fluted tubes as indicated by the Nusselt modulus, $Nu/Pr^{0.4}$, as a function of the Reynolds number is shown in Fig. 1. The Nusselt number is defined as $Nu = hd_{hyd}/k$, where h is the conductance coefficient (Btu/hr-ft^2-^{o}F), d_{hyd} is the hydraulic diameter (ft.) and is equal to 4 x cross-sectional area (ft^2)/perimeter (ft.), and k is the thermal conductivity of the water (Btu/hr-^{o}F-ft.). The Reynolds number is defined as vd_{hyd}/ν, where v is the mean axial velocity (ft/sec) and ν is the kinematic viscosity (ft^2/sec). The Prandtl number is $Pr = c_p\mu/k$, where c_p is the specific heat at constant pressure and μ is the absolute viscosity. The Dittus Boelter correlation, $Nu/Pr^{0.4} = 0.023\ Re^{0.8}$, for a smooth tube is shown for comparison.

The ratio of the ordinates for the four curves shown in Fig. 1 to that of the smooth tube curve indicates the amount of heat transfer enhancement achieved on the inside of the helically fluted tubes relative to a smooth tube. These curves do not include the effect of the extended area of the helically fluted tubes relative to that of a smooth tube of the same cross-sectional area. This is an additional factor of 1.33 for the tube reported here; in some of the tubes under development the extended area is 1.6 greater than the area of a smooth tube of equal cross-sectional area. Curves 1, 3, and 4 are the results from tests conducted by Heat Transfer Research, Inc. (HTRI), on a 1-in.-o.d. tube that had flutes with a 30^o helix angle and was approximately 7 ft. long. (The helix angle is defined as the angle the helix makes with the tube axis.) Curve 1 is for cooling; that is, the direction of heat flow is radially outward. Hot water flowing on the inside of the tube was cooled by colder water flowing on the outside. Although enhancement is achieved in this mode of operation, it is less than in the other curves since the density gradient is stabilizing.

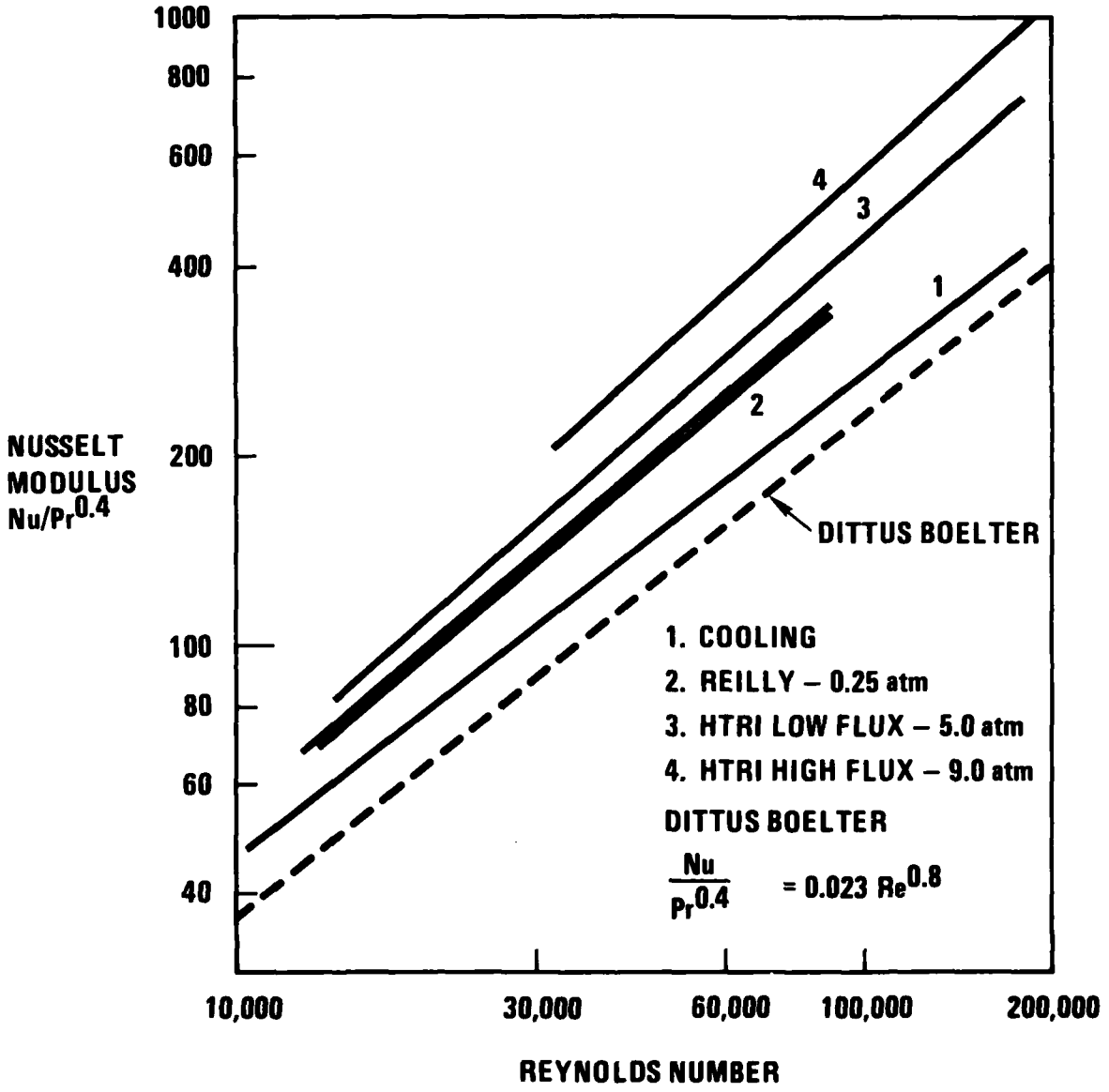

Fig. 1 Enhancement of 30° helix for varied heat flux

Curves 3 and 4, however, show significant enhancement. These data were obtained with the direction of the heat flow radially inward, which leads to density gradients that are destabilizing and hence increases turbulent exchange. Steam was condensed on the outside of the tube by colder water flowing on the inside. The condensing pressure was approximately 9 atm for curve 4 and 5 atm for curve 3 in these tests. The steam flow was parallel to the tube axis, which was horizontal. Data from two tests conducted by D. J. Reilly at the Naval Postgraduate School [2] on a 5/8-in. 30° helix angle spirally fluted tube are shown by curve 2. In these tests steam at 0.25 atm flowed transverse to the tube axis, which was horizontal. Curves 2, 3, and 4 indicate that as the condensing pressure and hence temperature were increased relative to the tube-side coolant, heat transfer increased. The higher condensing temperatures indicate higher heat fluxes and result in larger temperature gradients on the inside of the tube.

The frictional performance of the 30° helix angle tube can be seen in Fig. 2, where the isothermal friction coefficient (Moody definition) is plotted against Reynolds number for both the HTRI tests (indicated by the line and the Reilly tests (indicated by the triangles). The hydraulic diameter is used in the calculation for the frictional coefficient.

Since a decrease in the frictional coefficient in a tube in which enhancement of the heat transfer is achieved is surprising, a series of additional tests were undertaken. These experiments were designed to eliminate the uncertainties in the measurement of frictional coefficients in test rigs that were designed for heat transfer measurements. The preliminary data from the tests underway at the present time confirm the frictional coefficients depicted in Fig. 2 over a Reynolds number range between 40,000 and 80,000 with air as the fluid. Tests with water as the working fluid are scheduled which will also extend the Reynolds number range of the data. The cross-sectional area of the tubes varied from 0.127 $in.^2$ in the Reilly tests to 0.885 $in.^2$ in the tests underway at present. The cross-sectional area of the tube in the HTRI tests was 0.576 $in.^2$.

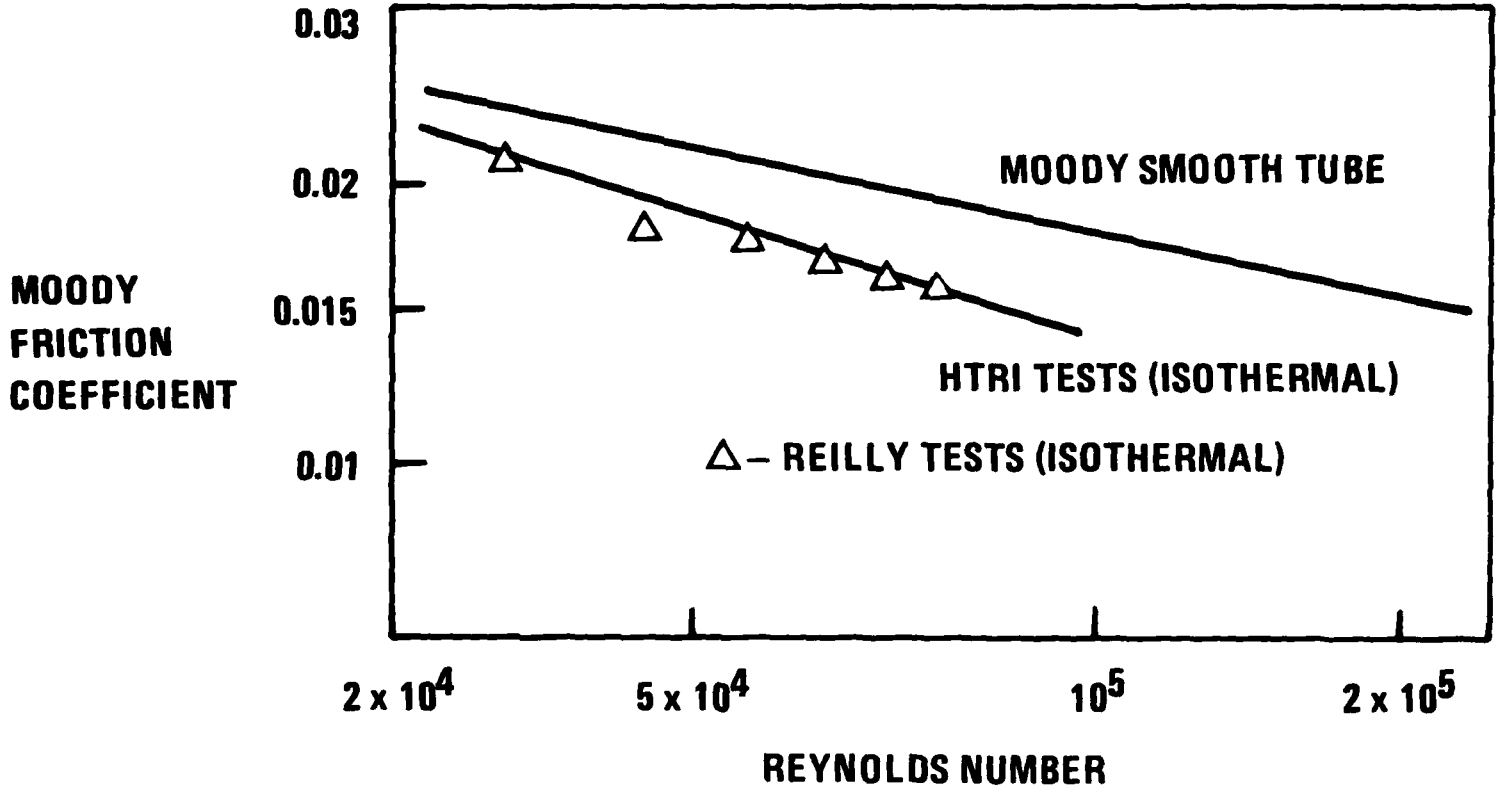

Fig. 2 Moody friction coefficient vs. Reynolds number for helically fluted tube

1.2 Combined Heat Transfer and Friction

While the analogy between momentum and heat transfer suggested by Reynolds and modified by Colburn is valid only under rather restrictive conditions, it is almost by definition an index of the degree of heat transfer enhancement achieved relative to the frictional penalty. It is directly related to the ratio of the exchange coefficients of heat to momentum. Therefore, it is of interest to examine the heat transfer and friction data in the context of the Colburn analogy. The Colburn analogy is defined as $2j/f^*$ and is equal to unity for a straight smooth tube, where $j = N_s Pr^{2/3}$. It is shown in Fig. 3 for the high flux case, the low flux case, the cooling case and for Reilly tests.

There are two items of interest. First, and least significant, is the positive slope that results from the negative slope of the friction coefficient/Reynolds number characteristics of Fig. 1, which is greater than that of a smooth tube. More important is the level of the Colburn factor, $2j/f$, which achieves a value of 2.3 at low flux and a value of 2.75 at high flux,when a value of one is the case for a smooth tube and less than one for most other enhancement techniques.

1.3 Condensation of Helically Fluted Tubes in a Vertical Configuration

Two tubes with different helical angles (one a 30° helix and the other a 45° helix) were tested at Oak Ridge National Laboratory with Refrigerant 11 condensing on the outside of the tube, which was cooled by water on the inside. The test data depicting the performance of these tubes are shown in Figs. 4 and 5. In Fig. 4, the condensing film coefficient is the ordinate and the heat flux is the abscissa. The increase in performance over the smooth tube decreases with heat flux

---

The frictional coefficients, f and f, used in the text and figures are respectively based on the Moody and Fanning definitions, which differ by a factor of 4. The Moody coefficient is larger than the Fanning coefficient by this factor.

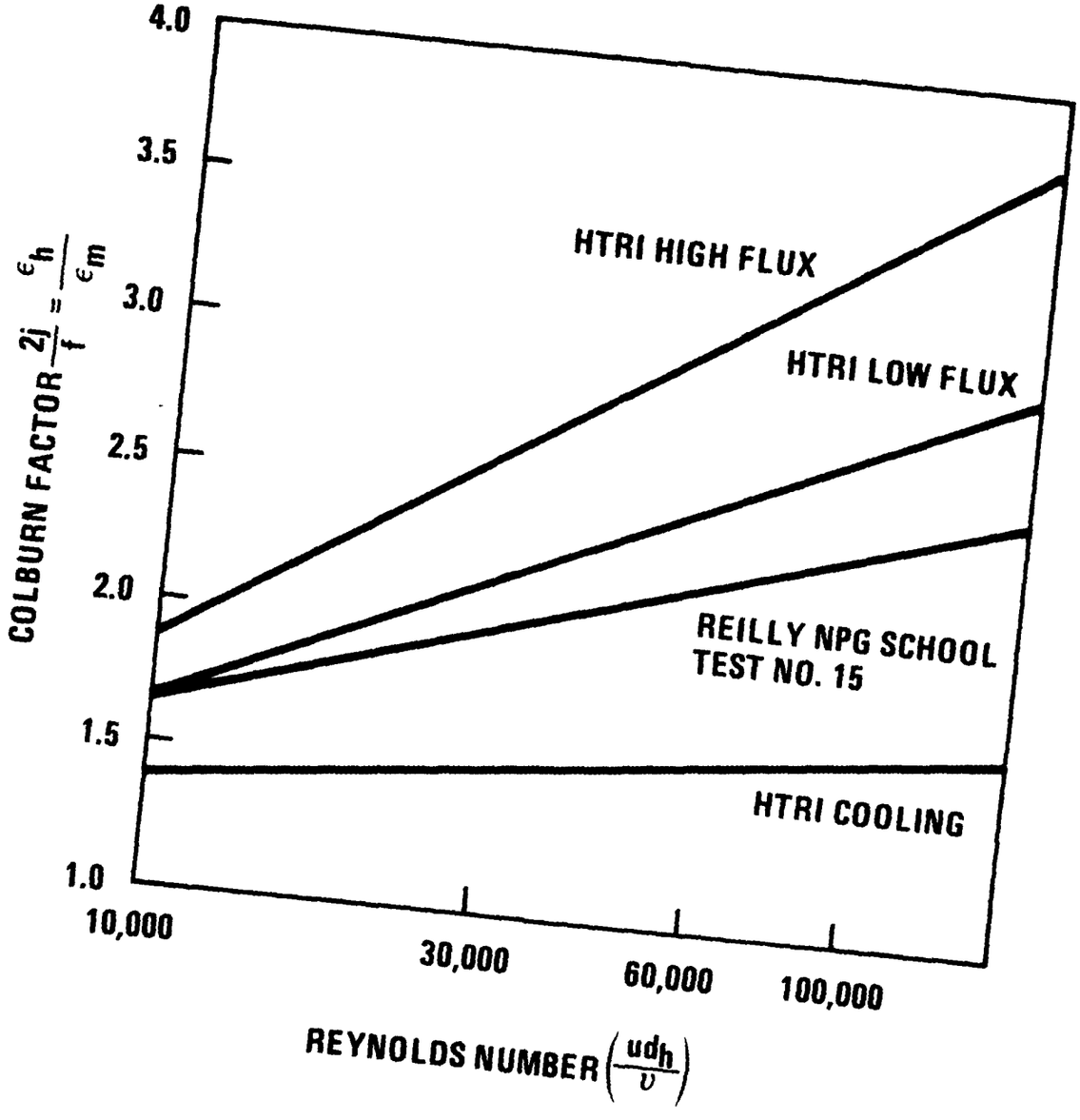

Fig. 3 Colburn Factor vs. Reynolds Number for helically fluted tube

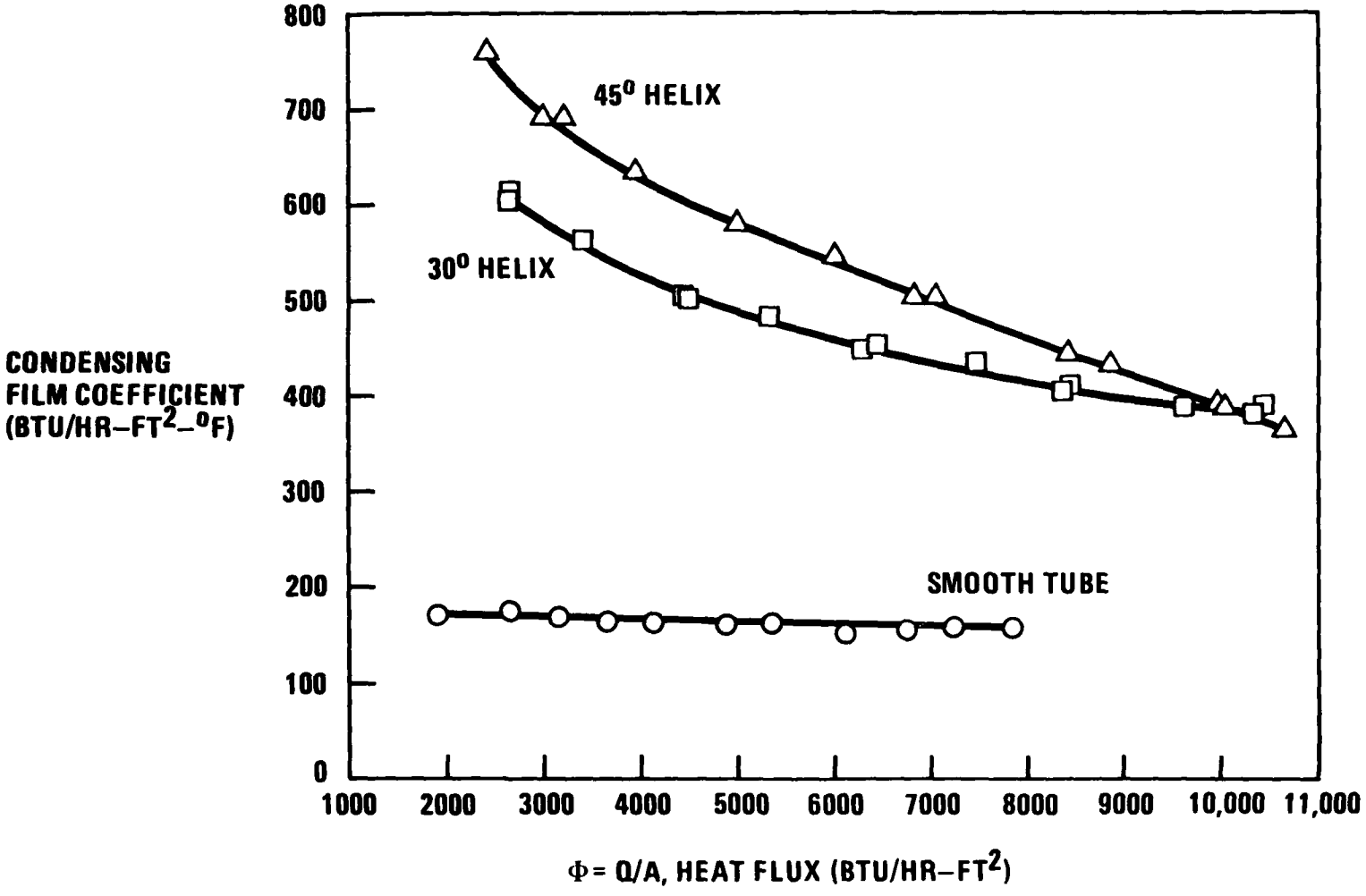

Fig. 4 Condensing film coefficient vs. heat flux for Refrigerant 11

but remains quite substantial. Figure 5 shows the same data with the heat load as the ordinate and the condensing temperature difference as the abscissa. Again, the gain over the smooth is larger at the lower heat loads. The 45° helix appears to have better performance at the lower heat flux. It should be pointed out that the 45° tube had fewer flutes and hence troughs, so the troughs would fill sooner. The liquid capacity of each of the flutes in both of these tubes was approximately the same. Therefore, a larger number of flutes would drain more liquid. Another fact that should be kept in mind is that the latent heat of Refrigerant 11 is quite low, so a considerably larger amount of liquid must be drained from the tubes than would be the case for steam or ammonia.

These data indicate that this tubing concept is uniquely suited to condensers, as enhancement is achieved in a vertical configuration on both the outside condensing surface and on the inside water surface without an increase in friction. These advantages can be particularly significant when the weight and volume of the condenser is important as it is in naval vessels either for the main propulsion system or for bottoming cycles.

Any rational explanation of the heat transfer enhancement that occurs without a frictional penalty must focus on the fundamental fluid mechanical processes of turbulence. It is widely recognized that the resistance to the transmission of heat (or any other scaler) from the wall to the internal flow in a tube is in the laminar sublayer adjacent to the wall where the process is dependent on the molecular conductivity. Improvements in the rate of radial heat transport resulting from increases in the turbulence level in the flow normally results in greater increases in the momentum losses relative to the increase in heat transfer. However, there are examples of instabilities in the atmospheric boundary layer that result in much greater heat exchange than momentum exchange. A laboratory experiment that illustrates the atmospheric phenomena is that of Mizushina, et al.[3] The exchange coefficients of heat and momentum in thermally stratified flow in an

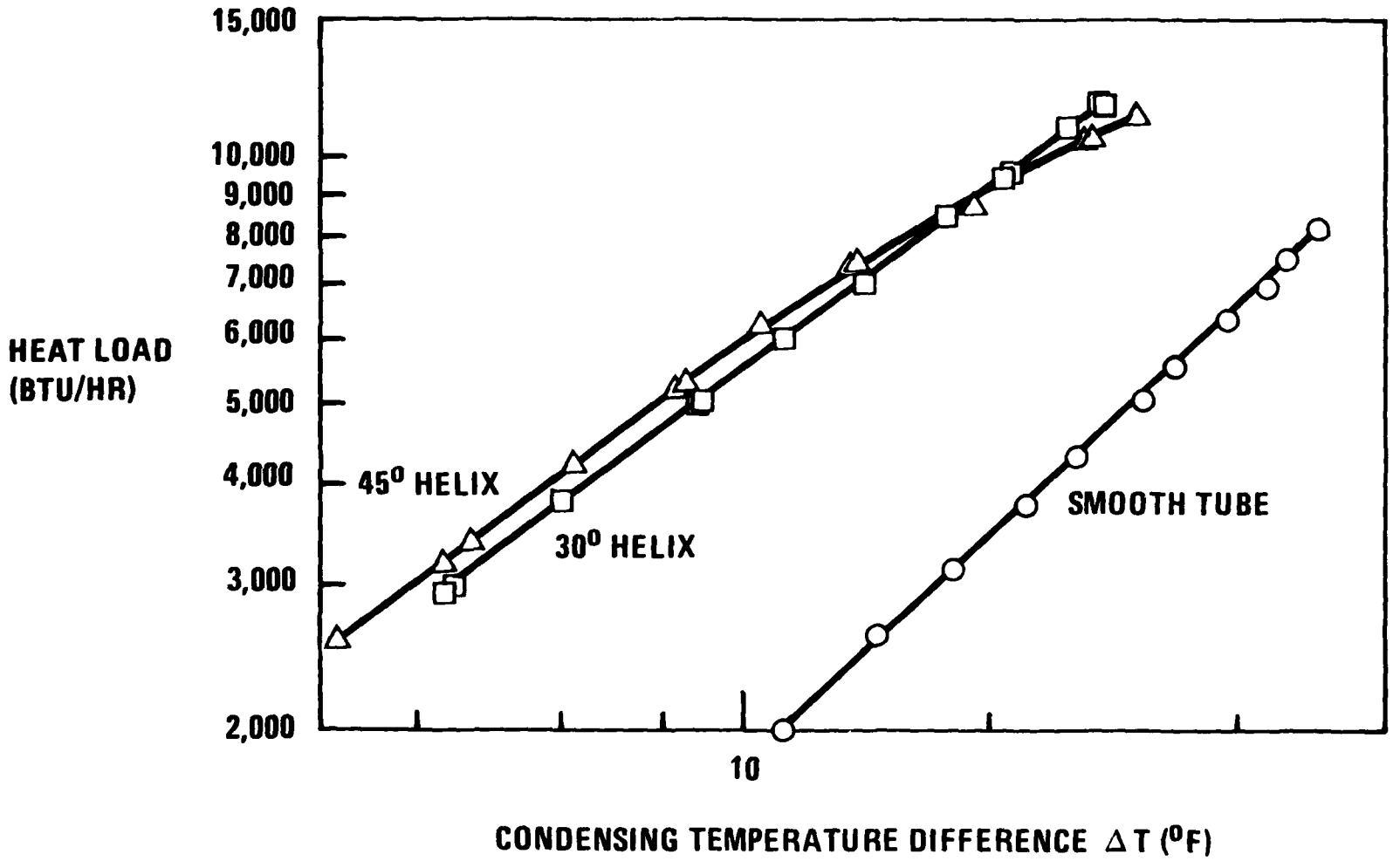

Fig. 5 Heat load vs. condensing temperature difference for Refrigerant 11

open channel under both stable and unstable conditions were determined from measurements of the temperature and velocity gradients. Their results indicate that the diffusivities of heat and momentum decrease with stability and the ratio of the diffusivity of heat to that of momentum decreases with increasing Richardson number. Under unstable conditions, the diffusivities of both heat and momentum increase with instability and the ratio of the diffusivities of heat to that of momentum increses to a maximum value of 3 as the stratification shifts from neutral to a weakly unstable condition. It then decreases gradually as the instability increases. It is our view that these effects of buoyancy in a gravitational field are replicated in the spirally fluted tube by the rotational flow induced by the flutes. There is an axisymmetrical core region, stabilized by swirl, surrounded by an annular region which is close to the flutes, highly three dimensional and unstable.

The purpose of this research program is to develop a theory to explain the increase in heat transfer relative to friction achieved in the reported measurements. A combined experimental and theoretical program has been underway at the University of California at San Diego and the General Atomic Company and is being expanded to include work at the University of Manchester and Imperial College. The initial work is reported herein and includes the construction of the experimental facilities, the development of a casting technique to provide a transparent test section which has an internal sprially fluted flow passage, the flow visualization studies performed to date, an experiment to measure the overall heat transfer coefficient using air as the cooling medium, the results to-date of the theoretical analysis and the work planned for the future.

2. EXPERIMENTAL PROGRAM

The foci of the experimental research effort during the past year have been the design and construction of both a water and an air flow facility. The water flow facility has been used primarily to study the flow field in a spirally fluted tube by means of flow visualization techniques, while the air flow facility has been used to determine the average or bulk heat transfer rates for air flowing inside the tube with the heat flowing radially inward. In the next sections we describe the two facilities as well as the major technological accomplishments in the development and construction of the two facilities. We next discuss the experimental results and the plans for future work.

2.1 Water Flow Facility

The water flow facility has been designed to provide a flow where the flow field in a spirally fluted tube can be studied both qualitatively and quantitatively. The facility is shown schematically in Fig. 6 and consists basically of a pump, damping tank, flow straightener, test section, and return line. The maximum flow rate corresponds to a Reynolds number in excess of 10^5 for a tube with a hydraulic diameter of 0.6-inch.

Since the flow facility is to be used initially for flow visualization studies, the test section has to be optically transparent, the inner surface must be goemetrically similar to the spiral fluted tubes which exhibit enhanced heat transfer, and the outer surface must be flat. The construction of such a test section is not a straightforward task and therefore has consumed a rather large percentage of our effort.

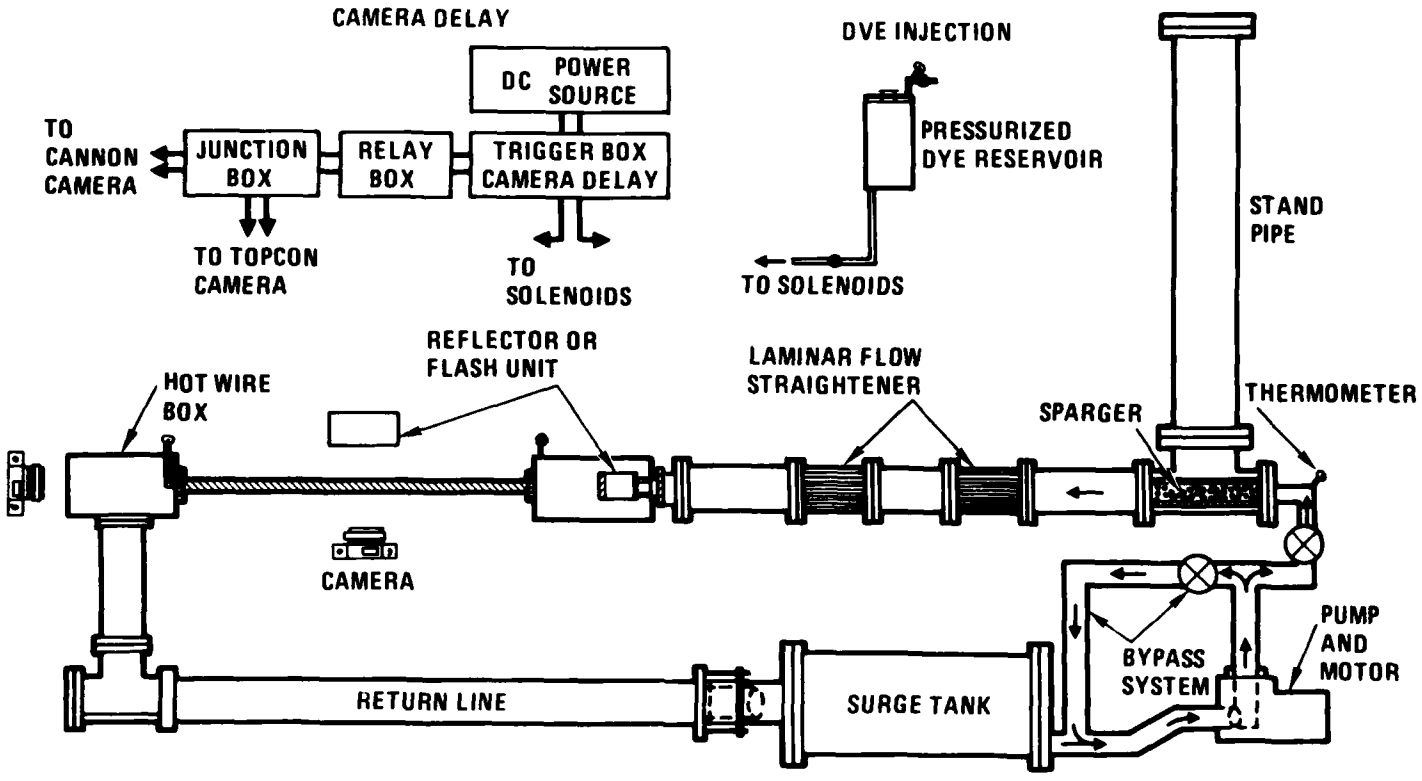

Fig. 6 Water tunnel

2.2 Test Section Construction

The transparent test section is constructed by placing an aluminum spiral fluted tube in the center of a 2.25 inch square mold. The sides of the mold are formed of 1/4 in. thick plate glass. The inside surface of the glass is covered with mylar film which is attached to the glass by means of double sided masking tape. A small, 1/8 inch slot, is left at the corner of two of the glass plates and the other corners are sealed with RTV rubber. It is through this slot that the resin is poured into the mold. The entire mold is filled with Castolite AP, acrylic-polyester resin. The hardening of the resin is slightly exothermic and is accompanied by some shrinkage - about 1/8" for each inch of thickness. Therefore it is important that the curing or hardening of the resin take place slowly and uniformly so as to lead to a minimum level of internal stress. This curing schedule can be accomplished by thorough mixing of the recommended minimum amount of hardener in the casting resin. Since the resin contracts during the hardening process, it must also be free to move relative to the boundary of the mold in order to reduce the magnitude of surface stresses and consequent surface cracking. It is for this reason that mylar which does not adhere to the resin is attached to the interior surface of the glass boundaries of mold. An alternate approach was developed in which the glass surface on the interior of the mold is coated with a light layer of hard wax but this technique yields a surface which is less transparent.

The shrinkage of the resin does lead to surface undulations with a peak to peak amplitude of 1/32 to 1/16 of an inch. These undulations lead to optical distortion and must be removed. The surface undulations are too large to be easily removed mechanically. For this reason, the hardened casting is placed in a second glass mold. The interior of the glass walls are covered with mylar as in the previous step and are placed about 1/8 inch from the surface of the casting. This thin layer is filled with casting resin. Shrinkage of this thin layer also occurs during hardening and leads to surface undulations with a peak to peak amplitude of 1/64 inch. These undulations can be

removed by wet sanding and then buffing with a polishing compound.

The exterior surface of the spiral fluted tube which is placed in the center of the mold is also treated so that the fluted, interior surface of the mold will be smooth and free of discoloration. This treatment consists first of machining the weld so that the weld becomes geometrically similar to a flute, second, of cleaning the exterior surface of the tube with a weak solution of sodium hydroxide, and, third, of buffing the tube surface.

After the resin from both pours has hardened, the glass is removed and the casting is immersed in a 30% solution of sodium hydroxide which is used to dissolve the aluminum tube. This process takes 2-3 days. The removal of the aluminum could be accomplished in a shorter period of time through the use of a more concentrated and/or heated solution. However, the heat release would be higher and would lead to a higher temperature of the casting resulting in discoloration.

Test sections up to eight feet in length have been cast. These long castings are mechanically strengthened by placing 1/4 inch diameter aluminum rods at the four corners of the mold which are fastened to plexiglas flanges at the two ends of the molds.

The test sections produced using the process described in the preceding paragraphs are of high optical quality which is required for the flow visualization studies and the possible quantitative measurement of the flow field by means of a laser doppler velocimeter.

2.3 Flow Visualization Studies

Flow visualization studies were made with the water tunnel shown in Fig. 6 with a four foot long test section that was produced using the casting technique previously described. Two plane mirrors were attached to the test section at approximately a 45° angle. Figure 7 shows the casting with the two plane mirrors. This enabled the observation of a top, bottom and side view from one side when the

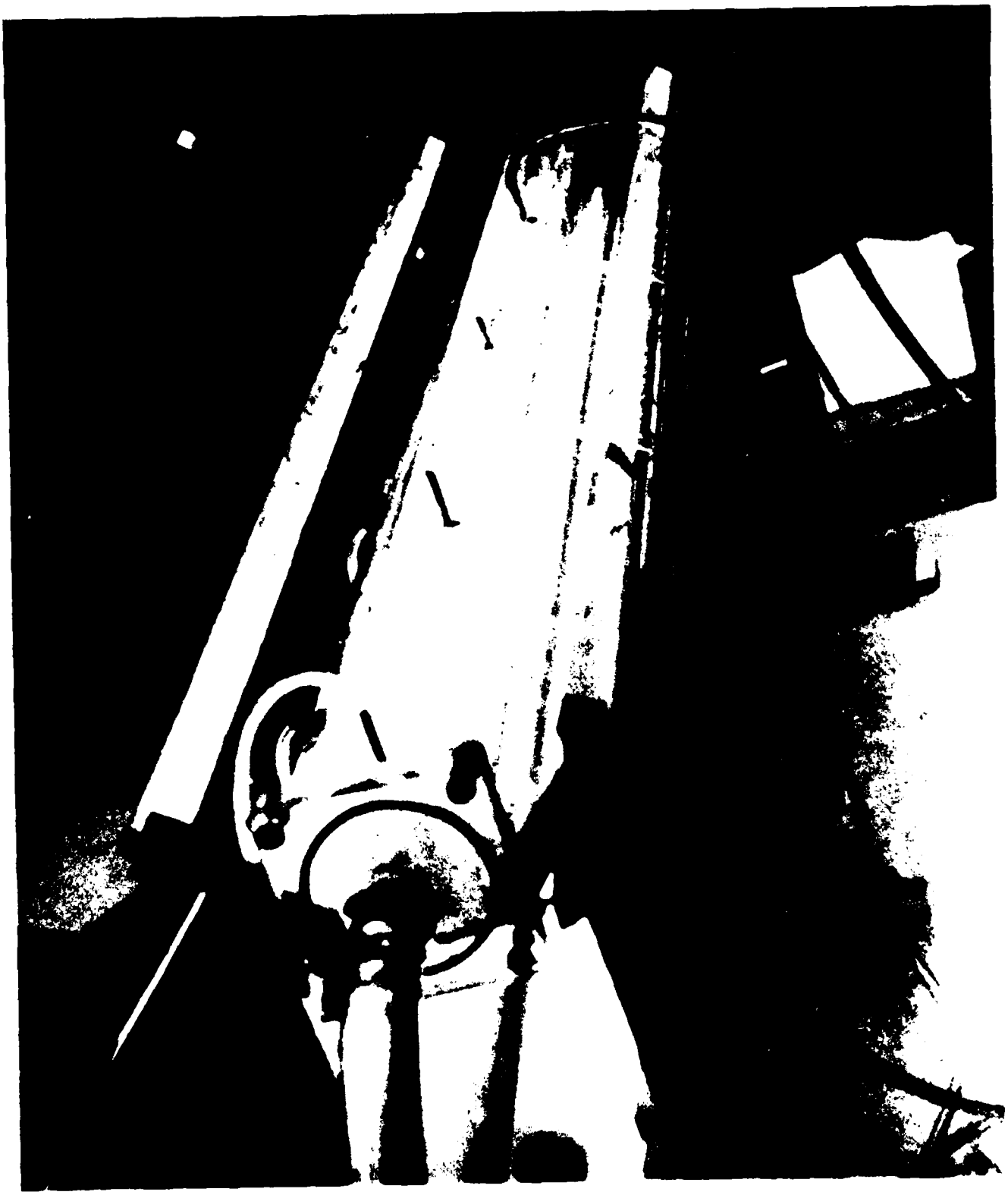

Fig. 7 Test section casting with plane mirrors at 45°

lighting source was from the opposite side. This turned out to be unsatisfactory as the light intensity was much greater in the direct view (side) than in the reflected views (top and bottom). The results were improved by introducing light through the back side of the test section and through one of the mirrors, the bottom one, and observing the top and side of the test section. Observations were also made through a transparent plate at the end of the water tunnel with illumination from the plenum section, upstream of the test section. Colored dyes, red and green, were introduced into the test section at five radial stations; wall (within the flutes), at the top of the flutes, at 1/8 diameter at 1/4 diameter, and in the center of the spirally fluted tube, 1/2 diameter. Both high speed motion and still photographs were taken. Figure 8 is a still photograph taken from the side of the test section. Red dye is injected at the top of the test section and green dye at the bottom with the water flow from the right to the left. The dye injection was continuous. The flute spiral is left handed and is curved from the bottom to the top and the far side of the test section can be seen as light hatching normal to the spiral on the viewers side. The rotational nature of the flow can be seen as the green dye rotates from its point of injection at the bottom toward the viewer and curves around the tube while the red dye, injected at the top, curves away from the viewer to reappear at the bottom approximately one pitch distance downstream. The two fluids appear to be completely mixed in two pitch lengths. The spiral angle is 30°, the tube diameter approximately 1 inch and the pitch approximately 5 inches.

End views of the flow in a spirally fluted tube can be seen in Figures 9 and 10. These are collages of individual photographs taken through the transparent downstream tunnel wall looking upstream into the spirally fluted tube. Lighting was provided by reflecting light from a mirror mounted in the upstream plenum section. Colored dye was injected into the tube through hypodermic tubes mounted on the sides of the transparent test section. A timing system was designed to inject the dye and then after a predetermined delay release the camera shutter. The system can accommodate two cameras, one viewing from the

Fig. 8 Flow visualization - side view. Red dye injected at top, green dye at bottom, water flow is from left to right.

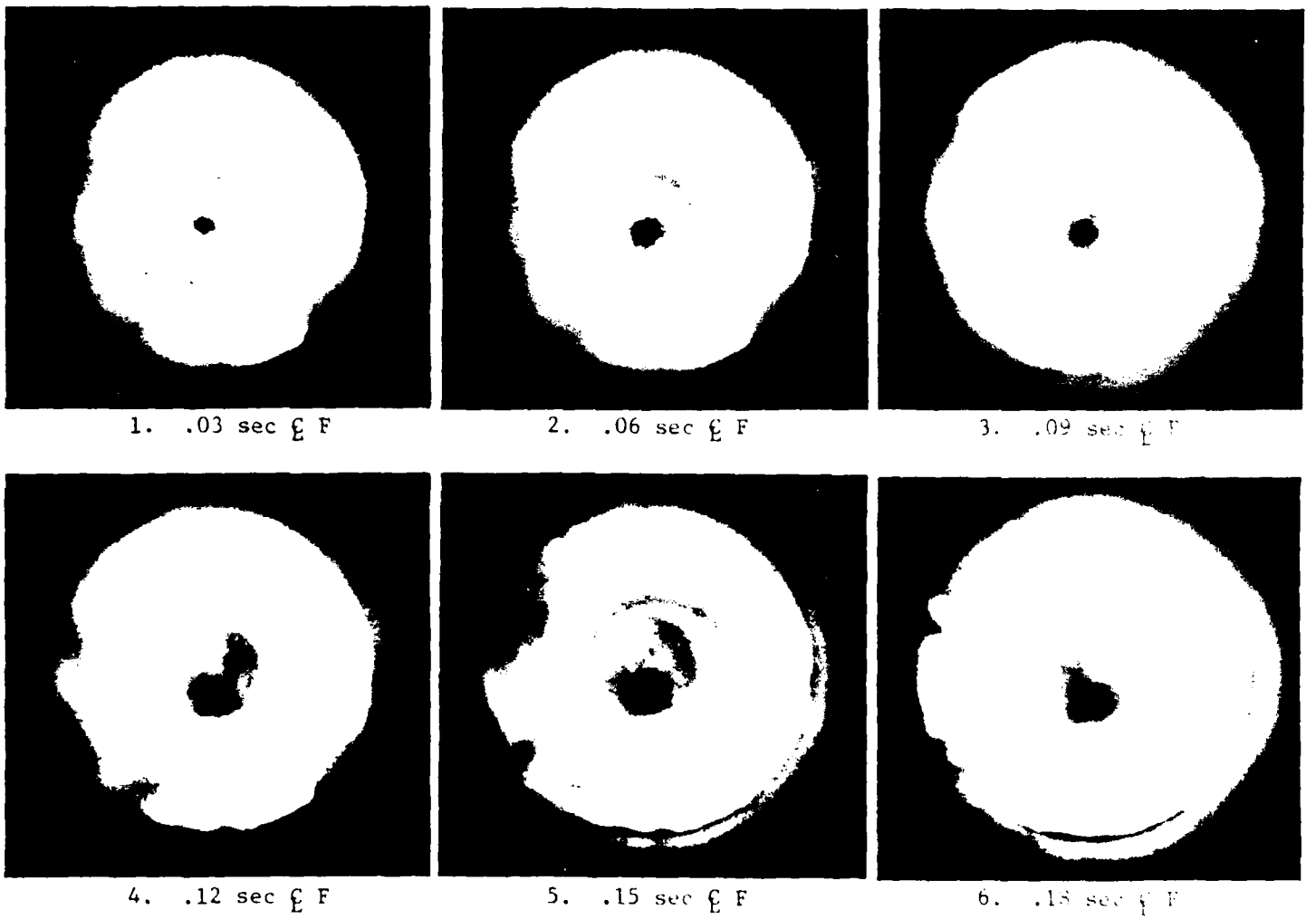

Fig. 9 Flow visualization sequential photographs, end view. Injection at centerline and plate top.

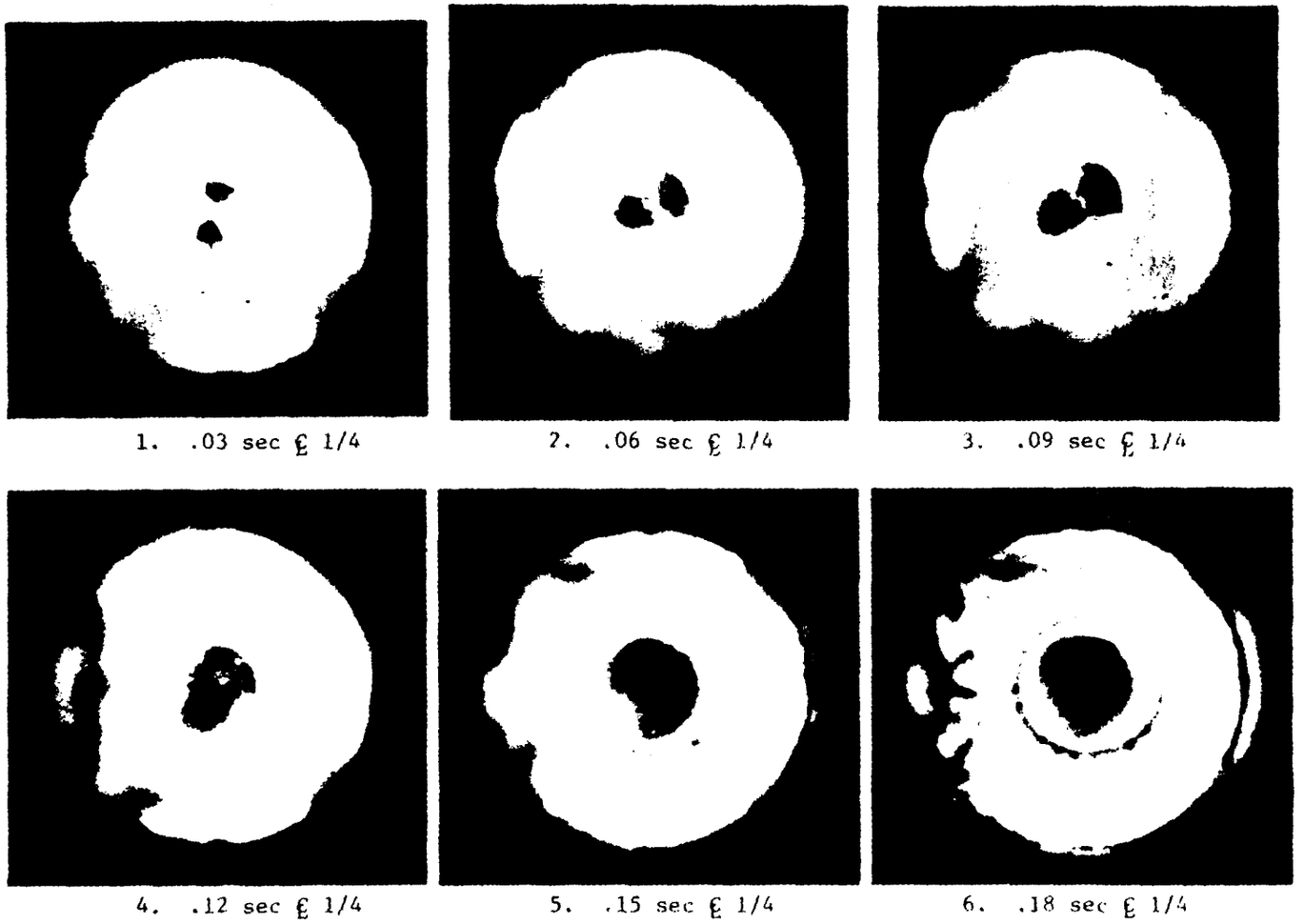

Fig. 10 Flow visualization, end view. Injection at centerline and 1/4 diameter.

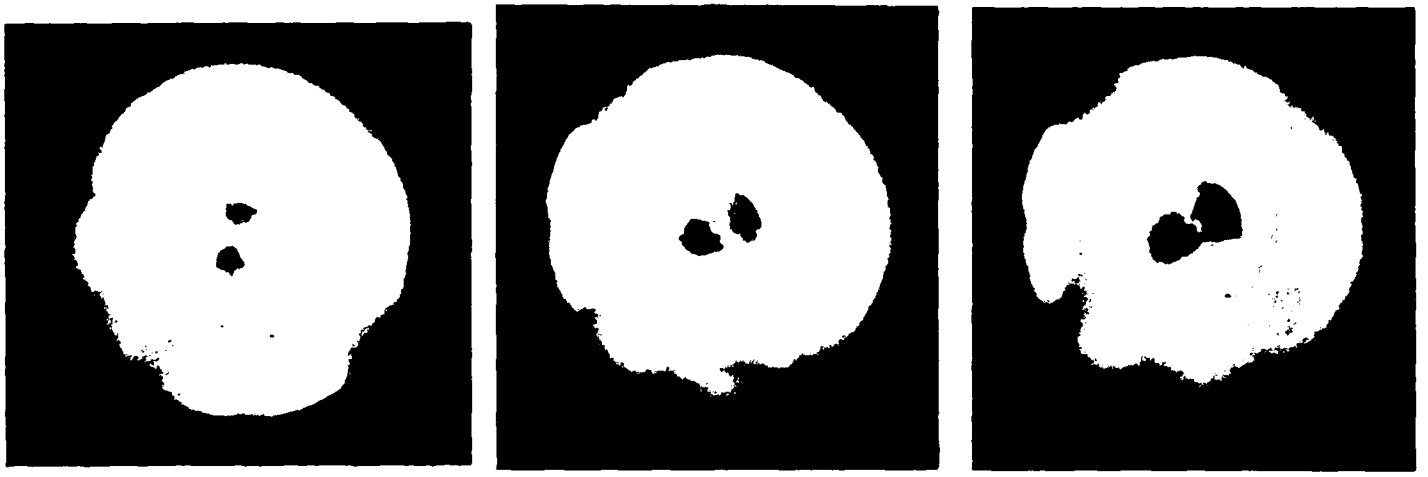

1. .03 sec ℄ 1/4 2. .06 sec ℄ 1/4 3. .09 sec ℄ 1/4

4. .12 sec ℄ 1/4 5. .15 sec ℄ 1/4 6. .18 sec ℄ 1/4

Fig. 10 Flow visualization, end view. Injection at centerline and 1/4 diameter.

end and the other from the side. A steady light source was used. Individual photographs were taken to simulate the fluid motion sequentially. Each photograph was taken with an individual injection of dye with a different time delay. The results taken to date are qualitative. In Figure 9 the injection of red dye was at the flute - core boundary and the green dye at the center line of the tube. Note the peripheral spread of the red dye as compared with the green dye particularly in picture 1 where the injections can be seen. (Rotation is clockwise.) In Figure 10 red dye injection is at 1/4 of the tube diameter and the green dye on the center line. In picture 1 of Figure 10 note the diffusion and rotation from the injectors. The rotation is not as marked as in the previous figure with red dye injection at the flute - core flow boundary. While these photographs, other still photographs, the high speed motion pictures and visual observations qualitatively support the notion of the flow rotation and turbulent exchange between the flute and core flows, they did not lead to definitive quantitative information. Since a steady light source of limited intensity was used, the exposure time and resulting resolution were limited. This proved to be a more severe handicap in the motion pictures. Furthermore, the inertia in the dye injection system leads to errors when sequential still photographs are compared. We anticipate that these problems will be resolved with the completion of the high intensity xenon flash system that is under development. This will enable high speed motion pictures with frame by frame flash synchronization with exposure times of less than 1/2 of a millisecond.

2.4 Quantitative Flow Measurements

A necessary synergism exists between the quantitative measurement of velocity and the theoretical model which will be used to predict the flow field. Thus, measurements of the velocity field in the spiral fluted tube are not only of fundamental interest but are also required to provide insight and guidance to the development of a valid theoretical model of the flow.

Two means of measuring the velocity are of interest: constant temperature anemometry and laser doppler anemometry. The latter offers several advantages in comparison to the former; the spatial resolution is better and the measurements obtained are neither contaminated by temperature fluctuations, nor by gas bubbles. Unfortunately, the cost of a laser system is about ten times that of the corresponding constant temperature anemometer system. The constant temperature anemometer system with spatial resolution of 1 mm is adequate in all regions of the tube except near the flutes. There, a laser system which can resolve scales to 0.2 mm, would have to be used. If measurements in the flute region become critical to the program, purchase of a laser system will be proposed. However, during the next phase of the research, we propose to make quantitative flow measurements by means of a hot film, constant temperature anemometry system. We next consider some of the problems associated with the use of the constant temperature anemometry techniques in water and then discuss the proposed measurements.

2.4.1 Measurement Problems in Water

The technique is based on the physical principal that the rate of heat transfer from a small heated cylinder is uniquely related to the velocity of a constant property fluid. In constant temperature anemometry the temperature of the heated cylinder, which consists of a thin layer of platinum which is sputtered on a 25μ diameter by 1 mm long quartz fiber, is held constant by appropriate electronic circuitry. The power required to hold the temperature constant is measured. The power depends on the velocity and on the surface conditions at the water-sensor interface which are unique to each sensor. Therefore each sensor must be individually calibrated - nominally on a daily basis - in a calibration tunnel where various stable flow velocities can be obtained. Contrast this with the laser doppler anemometer which maintains its calibration independent of the properties of the fluid.

A second problem encountered in hot film, constant temperature anemometry is outgassing of dissolved gas onto the surface of the film. This outgassing is due primarily to the facts that the sensor is

heated, that the surface serves as a nucleation site for dissolved gas, and that a relatively low pressure is created as the fluid moves around the cylindrical surface of the sensor. The occurrence of gas bubbles on the surface of the film dramatically effects the heat transfer rate and power required by the sensors. Thus great care must be exercised in removing dissolved gases from the water and removing those gas bubbles that collect at the sensor surface. Much of the dissolved gas can be removed by passing the water through a nozzle followed by a sudden expansion where suction is created. Gas bubbles can be blown off the sensor surface by means of a water or air jet and the occurrence of gas bubbles can be reduced by operating the sensor at a very low temperature.

However, as the operating temperature of the sensor is reduced, the sensor becomes relatively more sensitive to temperature fluctuations. Therefore, the temperature of the present water flow facility will have to be controlled.

Thus, the use of a hot film constant temperature anemometer will require the construction of a calibration facility which includes temperature control. Additionally, modification will have to be made to the existing water tunnel facility. These modifications include the addition of components to provide temperature control and removal of dissolved gas.

2.4.2 Proposed Measurements

We propose to measure the time resolved axial velocity component at various radial positions, at the exit plane of both a five foot and a ten foot tube. These measurements will provide a fundamental check of the model and also indicate with respect to only the axial velocity profile whether the flow is fully developed. We will also develop the instrumentation techniques that will permit the simultaneous time resolved measurement of both the axial and radial velocity components.

2.5 Heat Transfer Measurements in Air Test Rig

One of the objectives of this program that is necessary to obtaining an understanding of the fluid mechanics in the spiral fluted tube is the mesurement of the turbulence parameters of the flow field. At the onset of the program it was thought that this would best be accomplished with hot wire anemometry in air. However, the subsequent results of heat transfer measurements at HTRI showed considerable en ancement with water flow but not improvement with air. In both cases the direction of heat flow was radially inward. In the HTRI experiments, condensing steam at relatively high temperature was used as the heat source on the outside of the tube, and it was thought that the value of the Richardson Number was too negative. In the Mizushina experiments the ratio of the turbulent exchange coefficients of heat to momentum reached a peak of 3 at a slightly negative value of the Richardson Number and decreased as this parameter decreased. An alternate explanation of the different heat transfer behavior in gas as compared with liquid is in the viscosity variation with temperature. In gases the viscosity increases with increasing temperature, while in liquids it decreases. It was decided to examine this question in more detail by performing two additional experiments. The first experiment allowed the heat flux to be varied to include much lower heat fluxes than were achieved in the HTRI experiments. In the second, the direction of heat flow would be reversed to radially outward.

The first experiment was completed during the reporting period in an air test rig that was constructed and is shown in Figure 11. Filtered laboratory air was used as the test fluid in an open loop system. Steady air flow was provided to the test section by means of a centrifugal air compressor in line with a series of flow straighteners, a contraction section, and a 3-inch I.D. aluminum tube. Upon leaving the test section, the fluid expanded through a sparger tube into a second 3 inch aluminum tube, and was finally exhausted through a second

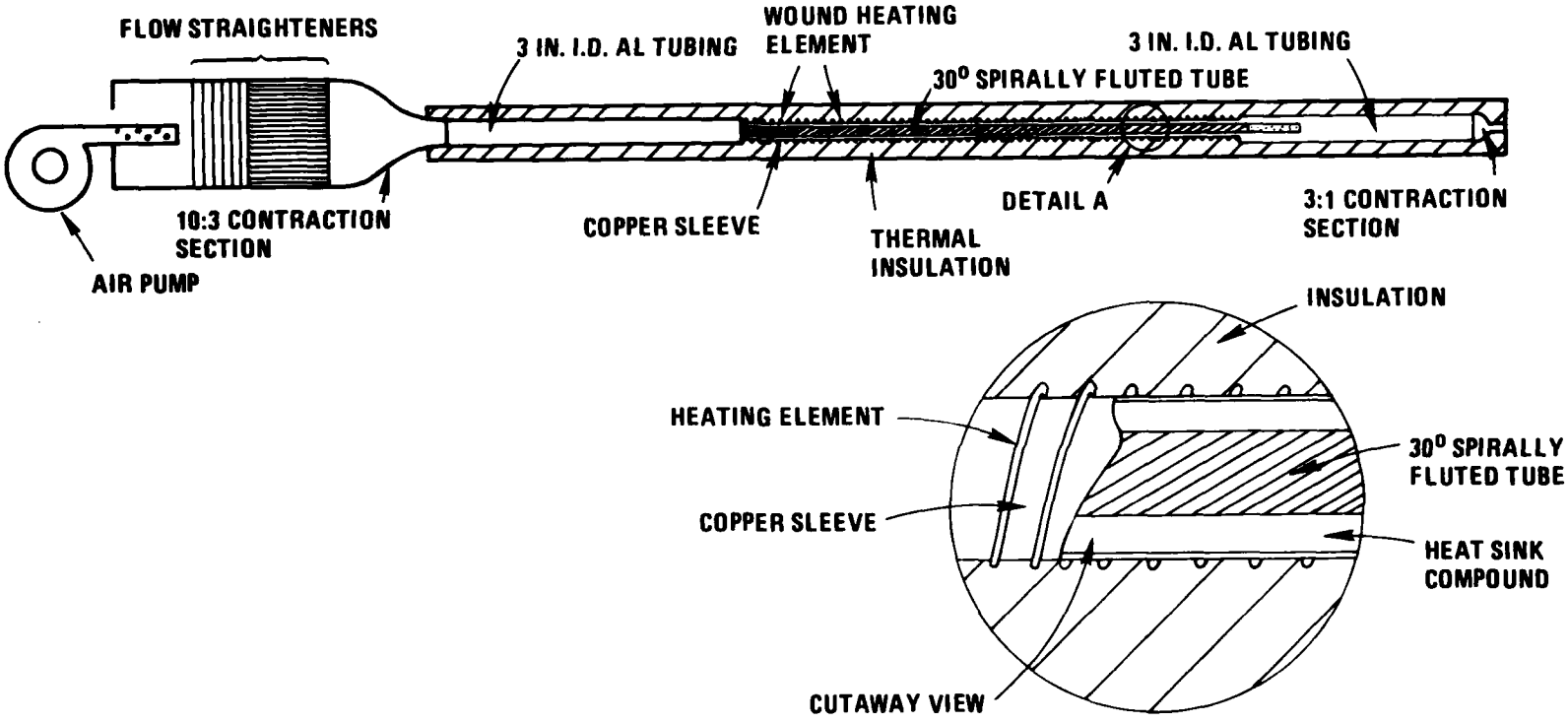

Fig. 11 Air test rig

contraction section. An inclined manometer was used to measure the pressure drop across the first contraction to obtain the flow rate, and a second manometer measured gauge pressure in the 3-inch tube, for determination of fluid density. The momentum and continuity equations were used to calculate fluid flow rates. Test fluid temperatures were measured with calibrated platinum resistance temperature probes, located at the entrance to the test section and at the system outlet. The outer surface of the spiral tube was packed with heat conducting grease and then installed inside a copper sleeve, which made complete contact with the grease. Test section heating was accomplished by wrapping the copper sleeve connected to a variable voltage source (0-240 volt) with a resistance heating element (0-1200 watt). The heat sink, grease, and copper sleeve were used to smooth out the heat distribution delivered by the heating element. Voltage across the heater and current through it were measured for computation of power input. Special thermal insulation covered the experimental system from the first contraction section to the system exhaust. Temperature distribution along the outer surface of the spiral tube was measured by means of copper-constantan thermocouples, with a 32° reference, installed in opposing sets of two at a 6-inch intervals along the tube.

Data for three different heat input rates with 3 to 5 flow rates for each heat rate were manually recorded. These data included inlet and outlet test fluid temperature, thermocouple voltage output, manometer readings for pressure drop and pressure in the 3-inch section, and voltage readings for power input to the heater.

2.5.1 Data Reduction

The rate of heat input (Q) to the test fluid was calculated from the relation

$$Q = W C_p (T_2 - T_1) \qquad (1)$$

where W (lb/hr.) is mass flowrate of the test fluid, T_1(°F) and T_2(°F) are temperatures of the test fluid at the test section inlet and system outlet, respectively, and C_p (Btu/lbm°F) is the specific heat at

constant pressure of the test fluid. The difference between the rate of heat input calculated in equation 1 and that calculated from voltage-current measurements of the heating element gives an estimate of heat loss from the system through pathways other than the test fluid.

After an initial distance from the test section inlet, skin temperature of the tube increases linearly with longitudinal distance. An equation describing this linear relationship takes the form

$$t = mx + b \qquad (2)$$

where $t(^{o}F)$ = tube skin temperature

$x(ft)$ = distance along tube

A least squares fit of temperature data obtained from the thermocouples was used to determine the slope m and the intercept b.

An overall heat transfer coefficient U ($Btu/hr\text{-}ft^{2o}F$) can be obtained from the defining equation

$$Q = A\ U\ \Delta t_m \qquad (3)$$

where Q (Btu/hr.) = heat transfer rate (Eq. 1)

A (ft^2) = tube heat transfer surface area

$$\Delta t_m\ (^{\circ}F) = \frac{\Delta t_{in} - \Delta t_{out}}{ln\ (\Delta t_{in}/\Delta t_{out})} \qquad (4)$$

where Δt_m is the log mean temperature difference, Δt_{in} is the difference between the test section skin temperature (Eq. 2) and the test fluid bulk temperature at the test section inlet, and Δt_{out} is similarly defined at the outlet. Values of U were plotted in the form $1/U$ versus $1/v^{0.8}$, the standard Wilson plot technique,[4] where v is test fluid velocity in the tube. A least squares fit of the points was obtained giving the slope and intercept of the equation

$$1/U = mv^{-0.8} + b \qquad (5)$$

The value 1/U is actually a sum of thermal resistance due to the tube wall thickness and the fluid film thickness on the inside wall. The thickness of this film decreases with increasing fluid velocity. The intercept on the vertical axis of the Wilson plot, which corresponds to infinite velocity, represents the resistance of the tube wall and resistances outside the wall which in this experiment is the leakage heat. A new line can then be constructed parallel to the original plot but with intercept at the origin. This line is the resistance due to the fluid film alone, and is the inverse of the overall coefficient independent of the other resistance terms. Thus by setting the intercept b equal to zero in equation (5), the resulting equation takes the form

$$1/hc = mv^{-0.8} \qquad (6)$$

which is used to obtain h_c. This value is then independent of thermal resistances other than those caused by the structure of fluid flow inside the tube. Further, by taking a least squares fit in constructing the original plot, correction is made for the slight scatter of data resulting from variations in the rate of heat input as the flow rate is varied.

The Nusselt, Reynolds and Prandtl numbers are dimensionless quantities defined by

$$Nu = h\, D_h/k$$

$$Re = v\, D_h/v$$

$$Pr = c_p \mu/k$$

where k, v and μ are evaluated at mean bulk fluid temperatures. Experimental results were plotted in the form Nu* versus Re where

$$Nu^* = Nu/[Pr^{0.4}\{T_b/T_w\}^{0.5}] \ .$$

T_b is the arithmetic mean bulk fluid temperature, and T_w is the mean wall temperature. Finally, a correlation to the heat transfer performance of a smooth tube was given by the well known Dittus Boelter equation[5]

$$Nu^* = 0.023\ Re^{0.8}$$

The results are shown in Figure 12 where the Nusselt Modulus vs. Reynolds Number variation is shown for the three heating rates and the Dittus Boelter correlation is shown as a straight line. The data agree with the straight tube correlation with the HTRI data at the higher heating rates. Table 1 gives the tabulated values of the measurements and calculations.

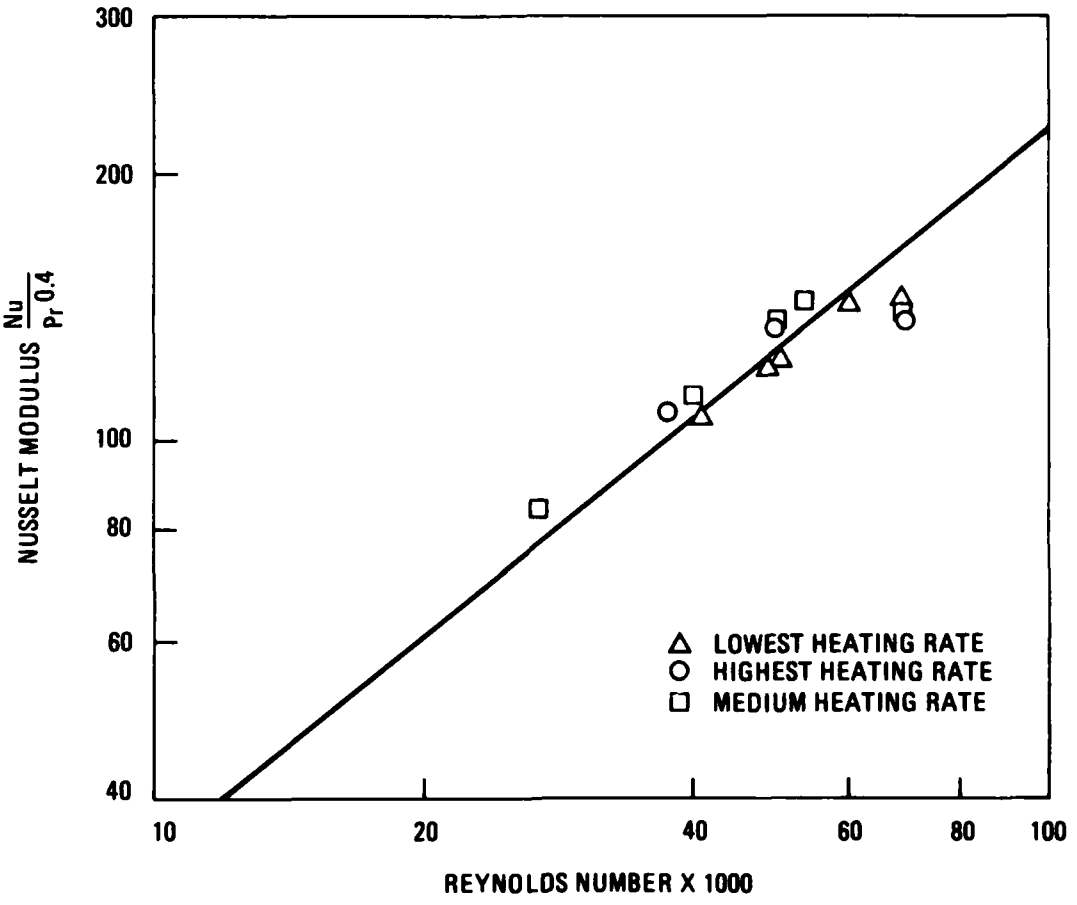

Fig. 12 Air test $\frac{Nu}{Pr^{0.4}}$ vs. Reynolds number

TABLE 1

HEAT TRANSFER AIR TEST

RUN NO.	GAS TEMPS (F) INLET	EXH.	CALC. HEAT INPUT (BTU/HR)	MASS FLOW (LBM/SEC)	VEL.-TUBE (FT/SEC)	RE #	LMTD (°F)	U_o (BTU/HR°F FT^2)	Nu	Tb	Tw	Nu*
52	95.02	111.10	688.87	.04950	168.32	48480.	15.02	32.30	103.9	563.06	578.26	121.24
54	85.81	105.72	713.05	.04137	138.85	40914.	18.92	26.54	90.2	555.77	576.00	105.66
55	120.99	132.19	698.75	.07195	254.90	68342.	11.49	42.83	123.9	586.59	596.62	144.07
57	96.96	113.09	709.63	.05080	173.35	49627.	15.46	32.32	106.0	565.03	580.50	123.72
58	108.09	121.36	713.08	.06200	215.22	59805.	12.86	39.05	124.2	575.13	587.8	144.72
59	101.28	133.19	1416.80	.05125	178.67	49272.	30.37	32.85	114.6	577.24	607.77	135.55
60	103.03	131.41	1362.31	.05542	193.20	53283.	27.07	35.44	122.0	577.22	604.72	143.95
62	94.79	132.62	1347.54	.04113	142.50	39720.	32.09	29.57	96.0	573.71	608.00	113.90
63	85.29	142.11	1374.48	.02793	96.77	26974.	46.74	20.71	70.4	573.70	620.5	84.38
64	126.73	147.95	1368.89	.07443	268.53	69736.	21.18	45.51	119.3	579.34	618.84	142.18
65	126.26	153.87	1760.89	.07358	266.67	68700.	28.12	44.10	117.0	600.06	624.00	137.54
66	102.92	135.56	1568.95	.05549	194.12	53208.	31.77	34.78				
67	97.43	136.41	1737.98	.05148	179.36	49509.	35.89	34.10	112.0	575.57	614.96	133.45
68	89.26	141.95	1774.09	.03888	135.15	37455.	47.34	26.39	90.1	575.60	622.95	108.05

3. THEORETICAL PROGRAM

3.1 Introduction

The spirally-fluted tube appears to have attractive features relative to enhanced heat transfer and thus to heat exchangers. In particular, the experimental data indicate increased heat transfer without a corresponding increase in pressure drop. From a fundamental point of view, these features call for an explanation of the mechanism by which the heat transfer at the wall is facilitated while the momentum transfer leading to pressure drop is not similarly increased. It is worth noting that analogous features are observed in geophysical turbulence where gravity provides a body force field corresponding to the centrifugal force field associated with swirl (cf.,e.g., Meroney [7]).* It is the purpose of this report to outline our current approach to the analysis of the flow within spirally-fluted tubing.

It will become readily evident as our discussion proceeds that the analysis of turbulent flow in such tubing cannot be fruitfully developed without an accompanying experimental effort providing detailed, accurate and extensive data on the statistics of the velocity components and subsequently of the temperature and the temperature velocity. Global measurements of heat transfer and pressure drop, the only measurements carried out to date in spirally-fluted tubing, are not sufficient to guide an analysis whose purpose is to provide more than correlations of experimental results, namely a fluid mechanical explanation of the transfer mechanisms involved. Such an explanation is necessary for the optimal design of such tubing.

---

*Meroney makes the following informative statement: "In the unstable case, a large flat heat flux is established quite rapidly, momentum transport may be significantly smaller in proportion.... It appears that buoyancy-generated eddies cause relatively little momentum transport, but they are quite effective at carrying thermal energy."

The need for experimental data is dramatically clear when the boundary conditions to be applied at the surface of the flutes are confronted. The flow within and immediately adjacent to the flutes must play an important role in determining tube performance. It is very complex and is being studied separately in the continuing work. Under these circumstances, such a role must be reflected in a modification of the "law of the wall," a modification which can only be determined by appropriate experiment. The possible importance of the wall region is indicated by the provisionally observed difference between tube performance with water versus air as the working fluid; the performance with the former appears to be significantly better than with the latter even within the same range of the parameters usually considered to determine flow behavior.

In an earlier study [8], we apply the results of So [9] to describe the fully-developed turbulent flow in tubing with spiral flutes. So assumes that in axisymmetric swirling flow, the various production and dissipative terms in the describing equations are so dominant that the equations are essentially satisfied by equating these terms. The results involve algebraic expressions for the turbulent exchange coefficients in the streamwise and radial directions. To utilize these relations, it is necessary to assume the radial distribution of a turbulent length scale. So argues that this scale is unaltered by swirl; thus in [3] we assume the standard length scale distribution $l(r)$ taken from [10]. In [11], So extends this approach to flows with heat transfer.

It is widely accepted that Reynolds stress closure represents the more complete formulation for turbulent shear flows and that as this closure methodology evolves, it will result in a standard procedure for engineering calculations applicable to such flows. Accordingly, in contemplating an approach for calculating not only the velocity field in spirally-fluted tubing but the thermal field as well, it appears that the full, second moment treatment of turbulent flows will provide a more general framework for the incorporation of experimental data than the analysis of So. The basis for such a treatment is provided by Launder and Morse [12] who apply

Reynolds stress closure to axisymmetric shear flows without and with swirl. Although it is possible to undertake a detailed assessment of the extensive modeling called for in their treatment, it is consistent with our view on the need for an evolutionary approach to accept their formulation as a starting point. In this regard, it should be noted at the outset that Ref. [7] is in the nature of a progress report; it indicates that in its present stage of development, the theory of axisymmetric shear flows is not adequate. Launder and Morse show that the spreading rate for nonswirling jets is predicted to be 50% too high. In addition, with swirl the shear stress ". . . $\overline{uw}$ has the wrong sign and thus the numerical solutions display a reduced rate of spread in contrast to the strong augmentation found in practice." These shortcomings suggest the difficulties of predicting swirling turbulent flows and the importance of close coordination between experimental and predictive efforts. We thus adopt the view that despite current deficiencies, the theory can in due course evolve to provide a useful predictive capability.

As a further justification for our adopted approach, we note that second-moment closure exposes in a clear fashion the mechanism whereby swirl affects the heat transfer characteristics of the tube. We find that the term $\overline{\theta'^2}\partial\bar{p}/\partial r$, the product of the intensity of the temperature fluctuations and the radial pressure gradient describes that mechanism. It is interesting to observe that this term is the counterpart of the gravity term in the atmospheric boundary layer.

At present, attention focuses on analyzing the velocity field within the tube. The coupling with the temperature field is considered as a second step. This sequential approach implies that we deal with small rates of heating and cooling.

3.2 Analysis

Figure 13 taken from [8] shows schematically the flow and coordinate system considered. We assume the flow is of constant density and fully-developed, i.e., only the mean pressure $\overline{p}$ varies in the streamwise direction. We follow the practice in [8] and [12] and denote the mean velocity components by capital letters and the related fluctuations by lower case letters. Thus, the mean velocity components of interest are U(r) and W(r) with fluctuations u and w. Although the mean radial velocity is zero within the core of the tube, its fluctuation v plays an important role.

3.2.1 Describing Equations

With these assumptions, preliminary work indicates that we must consider the following equations resulting directly from [12]:

Conservation of $\overline{u^2}$:

$$0 = -\frac{2}{3}\epsilon - c_1 \frac{\epsilon}{k}\left(\overline{u^2} - \frac{2}{3}k\right) - 2\left(1 - \frac{1}{3}(2\alpha - \beta)\right)\overline{uv}\frac{dU}{dr}$$

$$+ \frac{c_s}{r}\frac{d}{dr}\left(\frac{rk\overline{v^2}}{\epsilon}\frac{d}{dr}\overline{u^2}\right) \qquad (1)$$

Conservation of $\overline{v^2}$:

$$0 = -\frac{2}{3}\epsilon - c_1 \frac{\epsilon}{k}\left(\overline{v^2} - \frac{2}{3}k\right) - \frac{2}{3}(\alpha + 2\beta)\overline{uv}\frac{dU}{dr}$$

$$+ \frac{c_s}{r}\frac{d}{dr}\left(\frac{rk\overline{v^2}}{\epsilon}\frac{d\overline{v^2}}{dr}\right) - \frac{2c_s}{r^2\epsilon}\overline{w^2}(\overline{v^2} - \overline{w^2}) . \qquad (2)$$

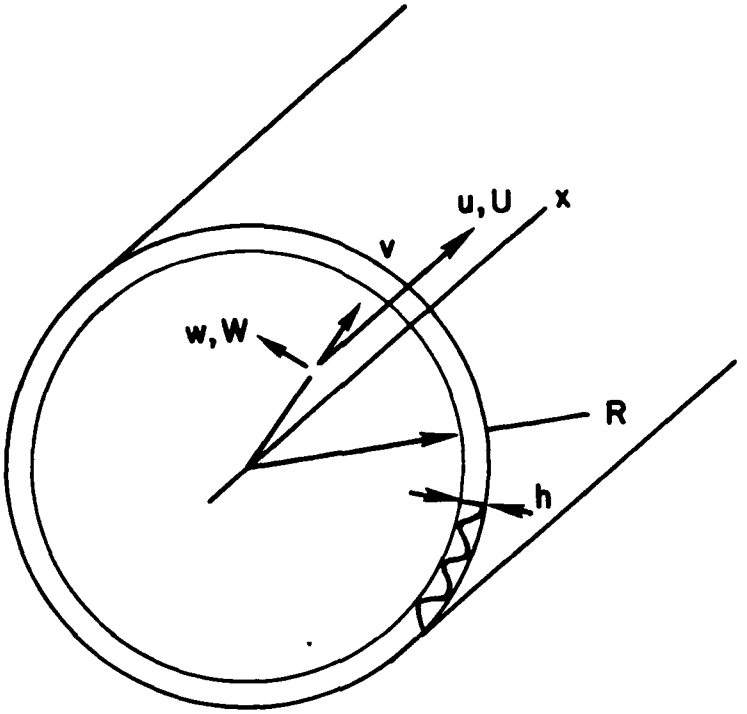

Fig. 13 Schematic representation of the flow and coordinate system

Conservation of $\overline{w^2}$:

$$0 = -\frac{2}{3}\epsilon - c_1 \frac{\epsilon}{k}\left(\overline{w^2} - \frac{2}{3}k\right) - \frac{2}{3}(\alpha+\beta)\,\overline{uv}\,\frac{dU}{dr}$$

$$+ \frac{c_s}{r}\frac{d}{dr}\left(\frac{rk\overline{v^2}}{\epsilon}\frac{d}{dr}\overline{w^2}\right) + \frac{2c_s k}{r^2\epsilon}\overline{w^2}(\overline{v^2} - \overline{w^2}) \qquad (3)$$

Conservation of $\overline{uv}$:

$$-\frac{\overline{uw}\,W}{r} = -c_1\frac{\overline{uv}}{k}\epsilon - (1-\alpha)\,\overline{v^2}\frac{dU}{dr} + \beta\left(\overline{u^2}\frac{dU}{dr}\right.$$

$$\left. + \overline{uw}\frac{dW}{dr}\right) - \gamma k\frac{dU}{dr} + \frac{c_s}{r}\frac{d}{dr}\left(\frac{rk\overline{v^2}}{\epsilon}\frac{d}{dr}\overline{uv}\right)$$

$$-\frac{c_s k}{r\epsilon}\overline{w^2}\frac{\overline{uv}}{r} - (1-\alpha)\,\overline{uw}\frac{dW}{dr} \qquad (4)$$

Conservation of ϵ:

$$0 = -c_{\epsilon 2}\frac{\epsilon^2}{k} - c_{\epsilon 1}\frac{\epsilon}{k}\overline{uv}\frac{dU}{dr} + \frac{c_s}{r}\frac{d}{dr}\left(\frac{rk\overline{v^2}}{\epsilon}\frac{d\epsilon}{dr}\right). \qquad (5)$$

In these equations, the notation is standard but several quantities call for comment. The quantity k is the turbulent kinetic energy $1/2\overline{u_k u_k}$ while ϵ is the velocity dissipation. The units of k/ϵ are (L/U) so that the coefficients in the diffusion terms have the units of (UL) as required.

We need additional equations to complete the formulation, but it is convenient to discuss Eqs. (1)-(5) before proceeding. In these equations, the following empirical constants appear: c_1; c_2 with the related constants $\alpha = (8 + c_2)/11$, $\beta = (8c_2 - 2)/11$ and $\gamma = (30c_2 - 2)/55$; c_s; $c_{\epsilon 1}$; and $c_{\epsilon 2}$. Values of these constants are given in [12].

In the absence of swirl, $W \equiv 0$ and Eqs. (1)-(5) represent five equations for the three velocity intensities, $\overline{u^2}$, $\overline{v^2}$, $\overline{w^2}$, the mean velocity U and the dissipation ϵ. Solutions to these equations subject to regularity conditions at the axis (r = 0) and boundary conditions at the wall describe the turbulent flow in either unfluted tubes or tubes with straight flutes. Clearly such solutions must be obtained as a first step in the development of our analysis.

The continuity and three mean momentum equations do not enter explicitly in our formulation; the first of these equations leads to $V \equiv 0$ while the x-wise momentum equation becomes

$$\frac{1}{4}\frac{d}{dr}\left(r\overline{uv}\right) = -\frac{1}{\rho}\frac{\partial \bar{p}}{\partial x} = \frac{\lambda \bar{U}^2}{R}$$

where $\lambda = 2\overline{uv}(r = R)/\overline{U^2}$ is the friction factor and $\bar{U}$ is the mean velocity defined by

$$\bar{U} = \frac{2}{R^2}\int_0^R Ur\,dr\,. \tag{6}$$

We thus obtain the radial distribution of Reynolds shear stress

$$\overline{uv} = \frac{1}{2} \lambda \overline{U}^2 \frac{r}{R} \tag{7}$$

so that $\overline{uv}$ is not a dependent variable in Eqs. (1)-(5). The radial momentum equation determines the radial pressure gradient after the characteristics of the velocity are known; we have

$$\frac{1}{4} \frac{d}{dr} \left(r \overline{v^2} \right) - \frac{W^2 + \overline{w^2}}{r} = - \frac{1}{\rho} \frac{\partial \bar{p}}{\partial r} . \tag{8}$$

As suggested earlier, Eq. (8) will enter significantly in the analysis of the thermal field in the tube but for the present may be set aside.

Finally, the aximuthal momentum equation leads to the important result that the Reynolds shear stress $vw \equiv 0$. We thus find that only two of the possible three shear stresses are operative in the flow under consideration.

With swirl one, additional equation is required, that for:

Conservation of $\overline{uw}$:

$$\frac{\overline{uv}\, W}{r} = - c_1 \frac{\overline{uw}}{k} \epsilon - (1 - \alpha) \overline{uv} \frac{dW}{dr} - c_1 \epsilon \frac{\overline{uw}}{k}$$

$$- \beta \overline{uv} \frac{W}{r} + \frac{c_s}{r} \frac{d}{dr} \left(\frac{rk \overline{v^2}}{\epsilon} \frac{d}{dr} \overline{uw} \right) - \frac{c_s k}{r^2 \epsilon} \overline{w^2}\, \overline{uw} \tag{9}$$

We must now take up the issue of the radial distribution of W; physical intuition suggests that within the central tube, there is a central core having a solid body rotation so that $W = \Omega r$ where Ω is a measure of the extent of rotation. This core region extends to the neighborhood of the flutes in the case of fluted tubing. Thus, the radius r = R takes on two meanings. For a smooth tube, R represents the interior radius. Such a tube may be fixed so that $W \equiv 0$ or rotating with an angular velocity Ω. Experimental results relative to the mean velocity distributions in the latter situation [13] and [14] indicate results similar to those predicted in [8], namely, profiles consistent with the stabilizing effect of rotation. The absence of turbulence measurements vitiates the value of these results.

For fluted tubes, the radius R should be considered R - nh as indicated in Figure 13 and is considered to determine the edge of the core involving rigid body rotation. The influence of the flutes on the flow is reflected in the boundary conditions to be imposed at r = R. The proper formulation of these conditions must be guided by experiment. With W(r) assumed given, Eq. (9) completes the system of six equations in six unknowns.

3.2.2 Boundary Conditions

The boundary conditions at the axis r = 0 are given by the physical requirements of regular behavior. We thus have:

$$\frac{d}{dr}\overline{u^2} = \frac{d}{dr}\overline{v^2} = \frac{d}{dr}\overline{w^2} = \frac{dU}{dr} = \frac{d\epsilon}{dr} = 0$$

$$\overline{v^2} = \overline{w^2}, \quad U = U_o, \quad \overline{uw} = 0 \tag{10}$$

In Eqs. (1)-(5) and (9), there are three intensities, the dissipation and the $\overline{uw}$-stress, each involving second derivatives, and the U-velocity component involving a first derivative for a total order of eleven. The

condition on (dU/dr) is automatically satisified if the other six conditions are applied so that there are four free quantities at r = 0 to be selected so that four boundary conditions at r = R can be imposed. We find it convenient to let $\overline{u^2}(0)$, $\overline{v^2}(0)$ and $\varepsilon(0)$ be three of the quantities in question with $\overline{w^2}(0) = \overline{v^2}(0)$ the fourth.

In contrast, the boundary conditions to be imposed at the edge of the core in order to reflect the influence of the flutes on the flow are uncertain. *Before* making even a provisional suggestion concerning the nature of these conditions, it is worth discussing several possible notions of the flow behavior in the neighborhood of the flutes. Suppose the resultant mean velocity due to the combination of the U- and W-velocity components is aligned with the flutes so that for $r \sim R \sim W \sim U \tan \phi$. Within the immediate vicinity of the flutes, both W and U decrease and approach zero. The distribution of azimuthal velocity within the flutes is thus destabilizing so that we think of the flute region as a region of high turbulence intensity tending to counteract the stabilizing influence of swirl in the core region.

If the resultant mean velocity in the neighborhood of the flutes is not aligned with the flutes, the flow will lead to further increases in turbulent intensities. This discussion suggests one obvious measurement, namely that of the radial distribution of the two mean velocities, U and W, with special attention devoted to the neighborhood of the flutes.

If we adopt the view that prediction of tube flow without swirl is the first order of business, the boundary conditions at r = R are clearly given by the law of the wall. In fact, this law provides a starting point for a provisional formulation which can be applied to fluted tubes pending experimental data leading to an improved description of conditions in the neighborhood of the flutes. Thus, we require as $r \sim R$

$$U \sim (\overline{uv})^{1/2} \left[A \quad n \left((R - r)\, \overline{uv}^{1/2}/\nu \right) + B \right].$$

By eliminating the distance from the core radius R - r, this equation can be rewritten as

$$U - (\overline{uv})^{1/2}\left[A \quad n\left(\frac{\overline{uv}\,A}{\nu(-dU/dr)}\right) + B\right] = 0\,. \tag{11}$$

Equation (11) assures that the velocity and the velocity gradient in the radial direction at the edge of the core are consistent with the log portion of the law of the wall. We expect that this equation may prevail even with swirl but are prepared to make modifications if experimental results so indicate.

The other two conditions to be imposed at r = R are more uncertain; the work of Launder et al. [15] suggests four possible choices, three relating $\overline{u^2}$, $\overline{v^2}$, and $\overline{w^2}$ to λ and a fourth relating ϵ to $\lambda\, dU/dr$. In the absence of guiding experimental data, we impose a condition on the intensity of the radial velocity fluctuations $\overline{v^2}$ since intuition suggests that the most direct influence of the flutes on the core flow is likely to be via that intensity. Thus, at r = R, we take

$$\overline{v^2} = \kappa_2\,\overline{uv} \tag{12}$$

where κ_2 is an empirical constant. As the final condition, we adopt the condition on the dissipation from [15], namely

$$\epsilon = -\,\overline{uv}\,\frac{dU}{dr}\,. \tag{13}$$

Although we have emphasized the provisional nature of the three boundary conditions at r = R, it should be noted that the general structure of the analysis, i.e., the availability of three quantities at r = 0 so that three conditions at r = R can be specified, is firm. Accordingly, other conditions can be imposed without altering, in a significant fashion, our analysis.

With swirl, we need another condition at r = R. If the mean flow at the edge of the core is taken to be tangent to the flutes, we have

$$W = U \tan \phi = \Omega R \,. \tag{14}$$

In connection with Eq. (14), we note that numerical analysis is facilitated if an inverse method is followed, thus we specify Ω and calculate a posteriori the appropriate flute angle ϕ.

3.2.3 Nondimensionalization and Reduction to First Order Equations

We use the centerline mean velocity U_o and the core radius R as the two nondimensionalizing quantities. Accordingly, we define the following dependent variables:

$$M_u = U/U_o\,, \quad I_u = \overline{u^2}/U_0^2\,, \quad I_v = \overline{v^2}/U_0^2\,, \quad I_w = \overline{w^2}/U_0^2$$

$$E = \epsilon R/U_0^2\,, \quad F_{uw} = \overline{uw}/U_0^2\,, \quad K = \frac{1}{2}\,(I_u + I_v + I_w) \tag{15}$$

In order to reduce the differential equations to first order, we introduce the following additional dependent variables:

$$G_u = \frac{\eta K I_v}{E}\, I'_u\,, \quad G_v = \frac{\eta K I_v}{E}\, I'_v\,, \quad G_w = \frac{\eta K I_v}{E}\, I'_w$$

$$G_{uw} = \frac{\eta K I_v}{E}\, F'_{uw}\,, \quad G_E = \frac{\eta K I_v}{E}\, E' \tag{16}$$

where prime denotes differentiation with respect to $\eta = r/R$, the single independent variable.

With the new variables, Eqs. (1)-(5) and (9) become:

$$I'_u = TG_u \tag{17}$$

$$M'_u \left[2(1-\alpha)\, F_{uw} + \frac{1}{3}\,(\alpha+\beta)\,\lambda\eta \right] - \frac{c_s}{\eta}\, G'_u = -\frac{2}{3}\, E - \frac{c_1 E}{K} \left[I_u - \frac{2}{3}\, K \right] \tag{18}$$

$$I'_v = TG_v \tag{19}$$

$$M'_u \left[\frac{1}{3}\,(\alpha - 2\beta)\,\lambda\eta \right] - \frac{c_s}{\eta}\, G'_v = -\frac{2}{3}\, E - c_1 \frac{E}{K} \left[I_v - \frac{2}{3}\, K \right]$$

$$- \frac{2c_s K I_w\,(I_v - I_w)}{E\eta^2} \tag{20}$$

$$I'_w = TG_w$$

$$M'_u \left[\frac{1}{3}\,(\alpha+\beta)\,\lambda\eta \right] - \frac{c_s}{\eta}\, G'_w = -\frac{2}{3}\, E - \frac{c_1 E}{K} \left[I_w - \frac{2}{3}\, K \right]$$

$$+ \frac{2c_s K I_w}{E\eta^2}\,(I_v - I_w) \tag{21}$$

$$M'_u \left[(1-\alpha-\beta)\, I_v + \gamma K \right] + \frac{1}{2}\, c_s \lambda\, \frac{K I_v}{E^2}\, E' = -\frac{1}{2}\, c_1\, \frac{E\lambda\eta}{K}$$

$$+ \frac{c_s \lambda}{2\eta} \left[\frac{G_v}{I_v} + \frac{G_u + G_v + G_w}{2K} \right]$$

$$+ \tilde{\Omega} \left[\frac{1}{2}\,\lambda\eta + (1-\alpha-\beta)\, F_{uw} \right] \tag{22}$$

$$F'_{uw} = TG_{uw} \tag{23}$$

$$\frac{c_s}{\eta} G'_{uw} = \frac{1}{2} \lambda \eta \tilde{\Omega} (2 - \alpha + \beta) + \left(\frac{c_1 E}{K} + \frac{c_s K I_w}{E \eta^2} \right) F_{uw} \tag{24}$$

$$E' = TG_\epsilon \tag{25}$$

$$\frac{c_\epsilon}{\eta} G'_\epsilon - \frac{1}{2} \lambda \eta c_{\epsilon 1} \frac{E M'_u}{K} = c_{\epsilon 2} \frac{E^2}{K} \tag{26}$$

where $T \equiv EI_v/\eta K$ is a dimensionless transfer coefficient and $\Omega \equiv \Omega R/U_o$ is a dimensionless swirl parameter. These equations are to be solved subject to boundary conditions at $\eta = 0$:

$$G_u \propto \eta^2, \quad G_v \propto \eta^2, \quad G_w \propto \eta^2, \quad G_\epsilon \propto \eta^2$$

$$I_v(0) = I_w(0), \quad M_u = 1, \quad \overline{uw} \propto \eta, \quad G_{uw} \propto \eta \tag{27}$$

and at $\eta = 1$:

$$M_u - \left(\frac{1}{2} \lambda \right)^{1/2} \frac{\bar{U}}{U_o} \left[A \quad n \left(\left(\frac{1}{2} \lambda \right) \frac{\bar{U}}{U_o} \frac{N_R}{(-M'_u)} \right) + B \right] = 0$$

$$I_v = \frac{\kappa_2}{2} \lambda \frac{\bar{U}^2}{U_\delta^2} \tag{28}$$

$$E = -\frac{1}{2} \lambda \frac{\bar{U}^2}{U_\delta^2} M'_u$$

where $N_R \equiv \bar{U} R/\nu$ is the usual Reynolds number based on the mean velocity.

The solutions to these equations depend on parameters λ, N_R and Ω and on various empirical constants which we can assume to be known but subject to adjustment to bring prediction and experiment into agreement. The specification of a value for λ calls for further empiricism relating the pressure drop characteristics to the Reynolds number, e.g., to $\bar{U}R/\nu$, and to the flute geometry, i.e., to the height, pitch, and spiral angle of the flutes. In [3], we use the pressure drop equation due to Blasius written in terms of the hydraulic radius and relate that radius to the flute geometry. The same treatment can be applied to the present analysis so that we compute as part of each solution the ratio $\bar{U}/U_o$ using Eq. (6).

3.2.4 Strategy of Solution

The numerical solution of this imposing set of eleven differential equations involving eight boundary conditions at $\eta = 0$ and three at $\eta = 1$ clearly involves two-point boundary values. We propose to use the method of quasilinearization to obtain the solutions. In this approach integration of the full, nonlinear equations with assumed values of $I_u(0)$, $I_v(0)$ and $E(0)$ plus three homogeneous equations obtained by quasilinearization is initiated at $\eta = 0$ and carried out to $\eta = 1$. The arbitrary constants which can multiply the solutions to the homogeneous equations are selected so that the boundary conditions at $\eta = 1$ are satisfied and so that the values of the guessed quantities are systematically improved. Convergence is achieved when no further improvements are called for.

3.3 Concluding Remarks

We have outlined an analysis applicable to the fully developed turbulent flow in tubes with spiral fluting. The general approach involves a second moment closure which is believed to provide a formulation permitting incorporation of essential experimental results. The importance of such results in the development of boundary conditions to be applied in the neighborhood of flutes is emphasized. The present analysis utilizes, in a

highly tentative way, conditions which complete the mathematical formulation and which have some physical content. However, we expect that these conditions will require modification when appropriate experimental results are available. Such modification can be incorporated in our general approach without difficulty.

4. CONTINUING WORK

The work on the experimental and analytical programs on the Fluid Mechanics and Heat Transfer of Spirally Fluted Tubing is continuing and will be reported on in subsequent reports. The principle areas are listed below.

4.1 Experimental Program

4.1.1 Flow Visualization Studies

The flow visualization studies are being directed toward obtaining quantitative data. As was mentioned earlier, this requires flash synchronization with a high speed motion picture camera. The elements of the system have been breadboarded and are awaiting the installation of the new cast section in the Water Tunnel.

4.1.2 Turbulent Measurements

Hot film measurements are planned in the water tunnel after completion of the flow visualization studies. Work is in progress on the calibration rig.

4.1.3 Heat Transfer Measurements with Air

A new air test rig has been designed and the parts manufactured for the measurement of the overall heat transfer coefficient with the direction of heat radially outward. The equipment is being assembled and the tests will be performed shortly.

4.2 Theoretical Program

4.2.1 Continuing Work

The analysis described in Section 3.0 is continuing and the programming of the equations is in progress.

4.2.2 Additional Theoretical Program

A subcontract has been issued to Prof. B. E. Launder at the University of Manchester to develop the methodology for the calculation of the flow field in and adjacent to the flutes. Work has started with contributions from Dr. A. D. Gosman of the University of London and Dr. Bergeles of the University of Athens.

ACKNOWLEDGEMENTS

The work done on this program was a joint effort between the General Atomic Company, (GA) and the University of California at San Diego, (UCSD). In particular, the experimental program was a collaboration between J. S. Yampolsky of GA and J. C. LaRue of UCI who jointly directed this phase of the work. The analytical program was accomplished by P. A. Libby of UCSD who acknowledges helpful discussions with B. E. Launder of the University of Manchester. During the course of this work there was considerable interaction and discussion among LaRue, Libby and Yampolsky.

The experimental program was accomplished by the following UCSD students in the areas noted.

P. B. Byers - Construction of the Air Test Rig, testing and report on the overall heat transfer measurements in air.

S. T. Hanyar - Assisted in flow visualization studies.

M. S. Layton - Flow visualization studies and contributions to the development of the casting of transparent test section.

L. M. Seckington - Casting of new transparent test section.

W. C. Stock - Manufacture, construction and initial operation of Water Tunnel. Development of photographic techniques.

The manufacture and construction was accomplished under the supervision of Ray Hummer of UCSD.

LIST OF SYMBOLS

Q	Rate of heat flow (Btu/hr.)
W	Mass flow rate (lbm/hr.)
Cp	Specific heat at constant pressure (Btu/lbm^{o}F)
t	Spiral tube outer wall temperature (^{o}F)
U	Overall heat transfer coefficient (Btu/hr-ft^{2o}F)
U_c	Corrected overall coefficient (Btu/hr-ft^{2o}F)
D_n	Hydraulic diameter (ft.)
K	Test fluid thermal conductivity
v	Kinematic viscosity (ft^2/hr.)
u	Absolute viscosity (lb/hr-ft.)
V	Average test fluid velocity (ft./hr.)

REFERENCES

1. Gregorig, R., Zeit. Agnew. Math. Phys. 5, 36-49 (1954).

2. Reilly, D. J., "An Experimental Investigation of Enhanced Heat Transfer on Horizontal Condenser Tubes," M.S. Thesis, Naval Postgraduate School (1978).

3. Mizushina, T., et al., "Buoyancy Effect on Any Diffusivities in Thermally Stratified Flow in an Open Channel," Proceedings of the Sixth International Heat Transfer Conference, Vol. 1, 91-96 (Paper MC16) (1979).

4. Wilson, E. E., "A Basis for Rational Design of Heat Transfer Apparatus," ASME, 47-83 (1915).

5. Welty, J. R., Engineering Heat Transfer, 1st Edition, John Wiley and Sons, Inc., New York (1974).

6. McAdams, W. H., Heat Transmission, 3rd Edition, McGraw-Hill, New York (1954)

7. Meroney, R. N., "An Algebraic Stress Model for Stratified Turbulent Shear Flows," Computers and Fluids 4, 93-107 (1976).

8. Libby, P. A., "Theoretical Analysis of Fully-Developed Turbulent Flow in a Spiral Fluted Tube," Department of AMES, University of California, San Diego, La Jolla, CA (1979).

9. So, R. M. C., "Turbulence Velocity Scales for Swirling Flows," in Turbulence in Internal Flows, Ed., S. N. B. Murthy, Hemisphere Publishing Corporation, Washington (1977).

10. Schlichting, H., Boundary Layer Theory, McGraw-Hill Book Company, New York, 502-514 (1960).

11. So, R. M. C., "The Effects of Streamline Curvature on Reynolds Analog," ASME Preprint 77-WA/FE-17 (1977).

12. Launder, B. E., and Moss, A., "Numerical Prediction of Axisymmetric Free Shear Flows with Reynolds Stress Closure," Turbulent Shear Flows I, Springer-Verlag, Berlin-Heidelberg-New York, 279-294 (1979).

13. White, A., "Flow of a Fluid in an Axially Rotating Pipe," J. Mech. Eng. Sci. 6, 47-51 (1964).

14. Murakami, M., and Kikuyama, K., "Turbulent Flow in Axially Rotating Pipes," J. Fluid Eng. 102, 97-103 (1980).

15. Launder, B. E., Reece, G. J., and Rodi, W., "Progress in the Development of a Reynolds-Stress Turbulence Closure," J. Fluid Mech. 68, 537-566 (1975).